Development of Wall Shear Stress Measurement Technique with a Thin Plate Submerged in the Sublayer

by Dan Hua

Graduate School of Sciences and Engineering

Yamaguchi University

2-16-1 Tokiwadai Ube, 755-8611

Japan

Abstract

We completed the development of a sublayer plate to measure both the wall shear stress in boundary layer and vector of the wall shear stress. We established design characteristics of the sublayer plate capable of measuring shear stresses in two and three-dimensional boundary layers, and also determines the calibration characteristics for various flow regimes by using experimental. These plates were then used to determine the flow characteristic in two and three-dimensional boundary layer.

A local wall shear stress measurement technique has been developed using a thin plate, referred to as a sublayer plate which is attached to the wall in the sublayer of a near-wall turbulent flow. The pressure difference between the leading and trailing edges of the plate is correlated to the known wall shear stress obtained in the fully developed turbulent channel flow. The universal calibration curve can be well represented in dimensionless form, and the sensitivity of the proposed method is as high as that of the sublayer fence, even if the sublayer fence is enveloped by the linear sublayer. The results of additional experiments prove that the sublayer plate has fairly good angular resolution in detecting the direction of the local wall shear stress vector.

A local wall shear stress vector measurement technique has been developed using a thin circular plate, referred to as a sublayer plate, which is attached to the wall in the sublayer of a near-wall turbulent flow. The pressure difference between the leading and trailing edges of the plate is correlated to the known wall shear stress obtained in the fully developed turbulent channel flow. A circular sublayer plate surrounded by eight pressure taps is designed to measure the wall shear stress vector. The curvature of the round edge of the circular plate slightly reduces the sensitivity to the wall shear stress magnitude in comparison with a rectangular plate. The circular plate can successfully detect the flow direction over a wide range flow angle. The circular plate with eight pressure taps has a higher resolution in the measurement of the wall shear vector using the ratio of the pressure differences at two taps adjacent to the tap showing the maximum stagnation pressure.

Contents

Chapter 1

Introduction

1-1 Background

The local wall shear stress is the most fundamental quantity when discussing the similarity of the turbulence in the wall layer of boundary layer, pipe, and channel flows. Knowledge of the wall shear stress is very important for many technical applications and for understanding all wall-bounded shear flows. The wall shear stress is caused by the viscosity of the fluid, which generates a thin boundary layer along the surface of the object. Due to adhesion at the wall surface, the local velocity within this boundary layer gradually increases from zero at the surface to a finite value of the edge and corresponds to an external flow where the viscous effect can be ignored. The magnitude of the shear stress depends on the velocity gradient and the viscosity of the fluid. An important process occurring in most fluid flows affecting momentum, heat and mass transport is turbulence. In this way, it plays a role in the generation of fluid friction

losses. The logarithmic mean velocity profile or similarity of the near wall turbulence is often used to determine the local wall shear stress for wall-bounded shear flows, provided that the similarities are independent of factors such as external forces or secondary currents. In engineering applications, the wall law and the defect law can be extended to more complicated situations, such as flows subjected to pressure gradients or three-dimensional flows. Shear stress near the wall acting in the direction of flow is commonly used as a design parameter for selecting and sizing countermeasures. The law of the wall must be validated in terms of the local wall shear stress as determined by a method independent of any similarity assumptions regarding the statistical properties. From a scientific and engineering point of view, wall shear stress is an essential quantity to calculate, measure, or estimate turbulence surrounded by walls. One of the most important results of the boundary layer theory is that the stress which was the determination of wall shear greatly determines the energy required to move the flow of liquid and gas over the solid wall. Therefore, knowledge of the magnitude and direction of the skin-friction vector and its distribution over a surface would be useful.

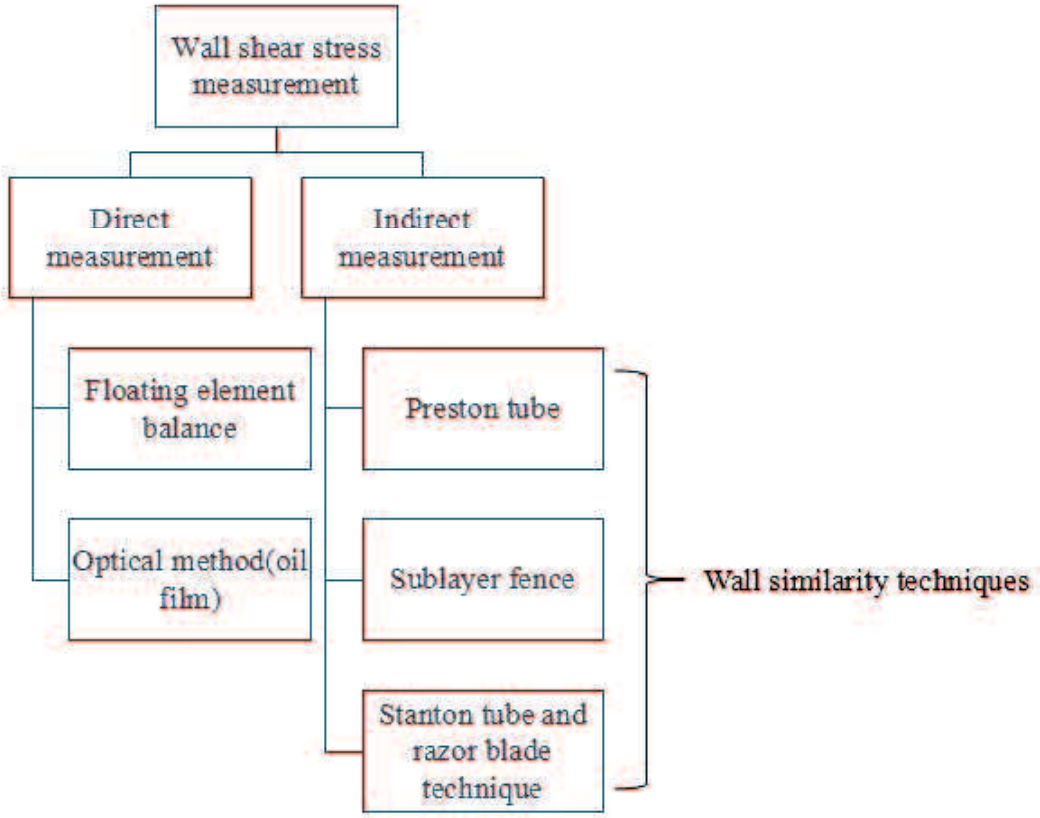

Fig.1-1 Classification of the main techniques for determining wall shear stress

Classical surveys for measuring the local wall shear stress have been proposed and used in several experimental studies on wall turbulence (e.g., Goldstein, 1983 and Winter, 1977), and, more recently, Hanratty and Campbell (1983) and Haritonidis (1989) presented review papers. Measurement techniques for the wall shear stress may be divided into a small group of direct methods (the floating element method and oil film

interferometry) and a larger group of indirect methods, which require calibration in well-known flows such as pipe flows or two-dimensional channel flows. In principle, direct measurement of the shear stress by force-sensitive surface elements is preferred as the calibration does not depend on the characteristics of the external flow. The floating element balance, which considers a large area and is very sensitive (allowing small forces to be determined), is probably the oldest method for measuring wall shear stress. This technology implies a large area and a very sensitive technique to determine small forces. It allows a very accurate measurement of the steady wall shear-stress values, about ±2%. The system frequency response is limited by the floating element size. The main drawback of the floating-element sensors is that they have poor spatial and temporal resolution for low-magnitude shear stress measurement, offers a shear-stress value, integrated over a larger or a smaller area and fails in providing exact pointwise measurements. To obtain a measurable output signal in a low-shear environment, a large sensing element is required, leading to a loss of spatial resolution. Hence it is not possible to simultaneously achieve a high sensitivity and high bandwidth. The drag balance technique can be applied to strictly limited situations and requires extremely sophisticated treatment (Allen, 1976 and Osaka, et al. 1997). The recently proposed oil film technique has been used in a boundary layer experiment at higher Reynolds numbers (Bandyopadhyay and Weinstein,

1991). This technique is based on the measurement of a oil drop's deformation, which is deposed on the test facility flow. The oil film is developed by drop's spreading due to the shearing. An accurate measurement of the mean wall shear-stress is acquired using this technique, being capable, in the same time, to measure reverse flow. The accuracy of the oil film method can be better, than within ±4%. Meanwhile, it is easy to apply and needs little instrumentation. Thus, a precise knowledge of the oil's viscosity is required. In other words, this technique requires careful arrangement of optical devices and considerably accurate oil viscosity values in the experimental setup. However, in practice, the direct measurement can be difficult to implement and is potentially subject to large errors under general flow conditions. Therefore, indirect shear stress measurement techniques have been developed.

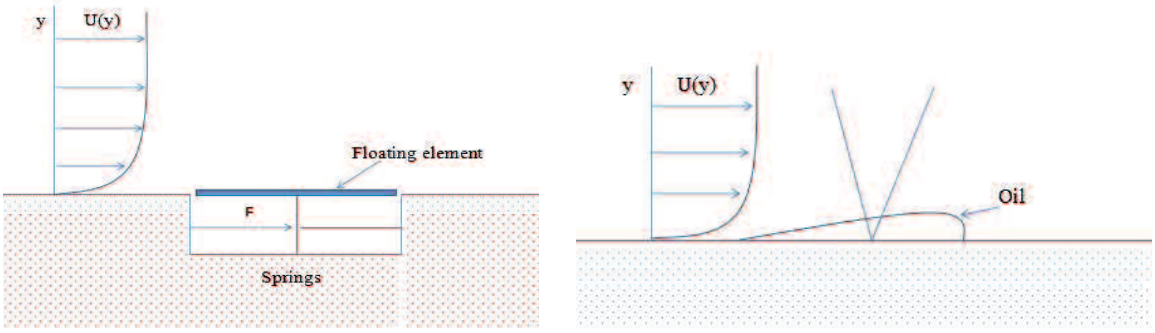

Fig.1-2 Main direct method of wall shear stress measurement: the left figure is the floating element method, the other one is the oil film interferometry

The Preston tube and the razor blade are simple and easily accessible devices that are applicable to many cases involving a flow over a smooth surface (Preston, 1954 and Patel, 1965). Preston tubes provide a convenient means of measuring the wall shear stress of two-dimensional turbulent flows because they are easy to make and use and are applicable over a fairly wide range of pressure gradients (Ghassem Zarbi and A. J. Reynolds). However, for cases in which the Preston tube is enveloped by a linear sublayer, the stagnation pressure is too low for accurate measurements at relatively low Reynolds numbers. Nowadays, there are some pressure measurement semiconductor devices that can detect small variations in the order of micro-pascal. However, most of these devices require impractical conditions such as small temperature variation in applications to experiment for aircraft or moving vehicles. The Preston tube is only one wall shear stress component, it is not a directional-sensitive.

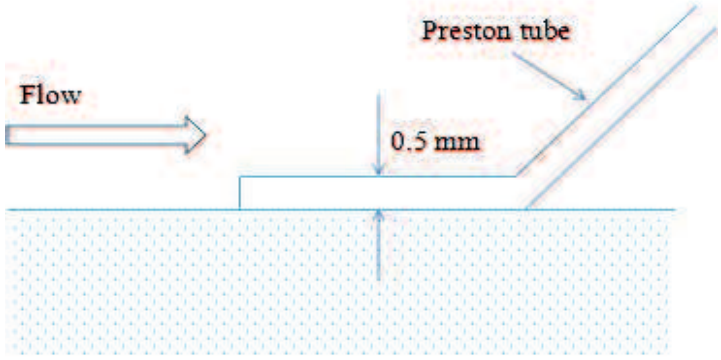

Fig.1-3 Preston tube: The wall shear stress is evaluated from the dynamic pressure at the opening of the probe

Sublayer fences generate a difference in pressure between the stagnation pressure in front of the fence and the pressure behind the fence, which enables more accurate pressure measurement if the fence is enveloped by the linear sublayer. However, each device must be customized and calibrated in canonical flows, such as channel or pipe flows. The pressure difference generated by fence are usually small and commonly only the mean value can be obtained, so there are serious questions about the use of the fence in situations where the instantaneous pressure difference varies very widely- as it does in separated flow region, for example. In addition, the sublayer fence is difficult to construct, primarily due to the narrow gap between fence elements and pressure taps. As such, the sublayer fence also requires customized sensors. Moreover, calibration curves must be prepared for each fence in canonical flows in which the wall shear stress is already known accurately. The primary disadvantage of the sublayer fence, however, is that universal calibration curves cannot be obtained for sensors fabricated in the laboratory.

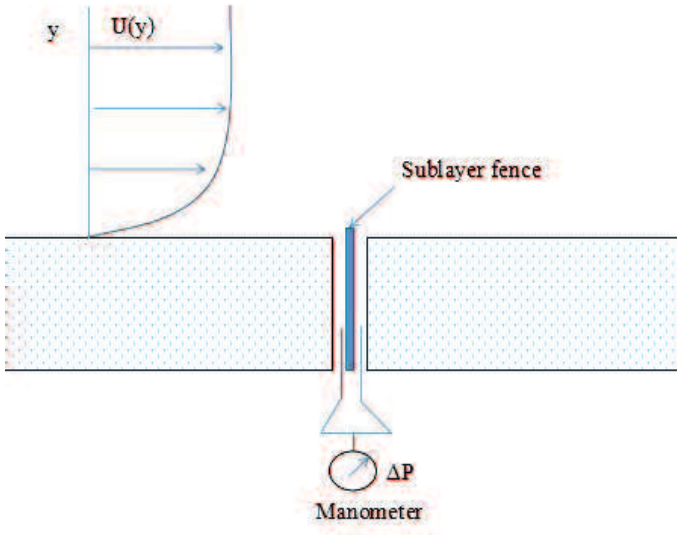

Fig.1-4 Wall shear stress measurement with the sublayer fence

The angular resolution of the wall shear stress measurement devices has been studied for widely known standard methods using a Preston tube and a surface block. Gupta (Gupta, 1975) introduced modified Preston tubes combined with a pitot-static tube as a device for measurement in a flow in which the flow direction is initially unknown. Dextor provided experimental evidence that the certain ratio of wall static pressure measured around a triangular surface block can resolve the flow direction for a considerably large range of angle of attack (Dextor, 1974). Hakkinen et al. used a multiple-tap cylinder embedded in the wall to measure the wall shear stress vector on an aircraft wing (Hakkinen et al., 2003). Analysis of the experimental data showed that the ratio of the differences in the static pressure at multiple pressure taps could provide a higher angular resolution for the wall shear stress vector measurement.

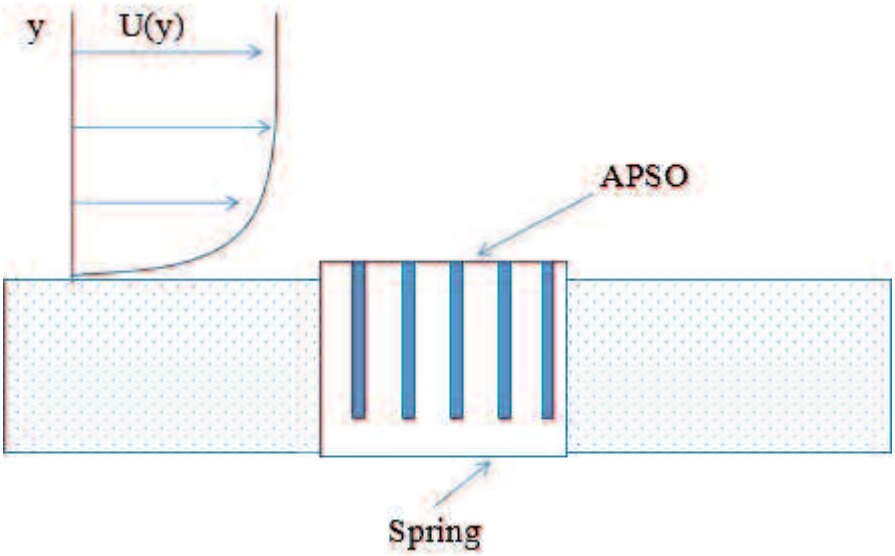

Fig.1-5 Schematic diagram of the adjustable-protrusion surface-obstacle (APSO) Skin Friction Vector Gage

1-2 Objective

Based on the above considerations, we herein propose a local wall shear stress measurement method using a simple device that is broadly accessible and that provides sufficient accuracy even when the device is enveloped by the linear sublayer. The sublayer plate technique is based on the similarity law. It contains two kinds of plate, one is the rectangular sublayer plate, the other one is the circular sublayer plate. The proposed device, which is referred to as a sublayer plate, consists of a thin rectangular plate and two static pressure taps on the wall. The measured differential pressure of the plate is correlated to the local wall shear stress assuming a relationship between this pressure and the velocity distribution

close to the wall. The plate can easily be fabricated to have the exact same size and shape and can be used to calculate the wall shear stress using a universal calibration curve. The sublayer plate also has the ability to detect the flow direction, namely, the direction of limited streamlines on the wall. In the present experimental study, the feasibility of using a sublayer plate to detect the flow direction with higher accuracy will be examined in a canonical two-dimensional turbulent channel flow. Considering the ratios of the static wall pressure measurement values, a circular sublayer plate with multiple static pressure taps will be used as the sublayer plate. The round edge of the plate could reduce the absolute values of the stagnation pressure at the upstream edge of the plate and the negative pressure at the downstream edge of the plate. The influence of the curvature of the round edge on static pressure measurement will be discussed, and, based on experimental results, we propose an arrangement of the plate and pressure taps that enables the flow direction to be determined with much higher accuracy.

The present work sets the following goals:

- Derivation of the governing relations
- Description of the capabilities of the available sublayer plate measurements in wind tunnel
- Design of an experimental setup suitable for the sublayer plate measurement

- Application of this measurement technique to various flow conditions
- Examine the angular resolution of the sublayer plate

Chapter 2

Facility and Equipment

2-1 Wind tunnel

The experimental work was performed in the Yamaguchi University Fluid Mechanics Laboratory wind tunnel which is shown in Figure 2-1. The calibration wind tunnel used in this study is a balloon type two-dimensional channel wind tunnel composed of a blower part, an enlarged part, a collecting part and a throttle part. For blower, the model SC-3 made by Nikui blower Co., Ltd. was used, and the maximum blowing volume is 198 m3 / min, the maximum static pressure is 50 mm Aq, the rotation speed is 935 rpm, the output is 3.7 kW. Also, in order to purify the inflowing air, a filter is attached to the intake port. Guide feathers were attached to the outlet part as a countermeasure against flow deflection and fixed on the frame of the wood for noise and vibration of the blower. The enlarged portion contracts 3.1° in the flow direction and is enlarged at 18.5° in the span direction. The area ratio of enlarged part is 1.7. Four sets of stainless steel rectifying wire gauzes with mesh 10, linear 0.605 mm, opening ratio of 0.58 were installed in the gathering

section to regulate flow. The throttle part is a two-dimensional throttle with a throttling ratio of 10, securing flow uniformity, and a parallel part is set at 40 mm nozzle outlet to reduce turbulence. The dimensions of the measurement part are the measurement part total length L = 6000 mm, the height 2H = 40 mm, the width D = 700 mm, the aspect ratio is 17.5 and satisfy the condition ARc> 7 for securing the channel flow two-dimensional nature by Dean (1978). In addition, the dimensions of the lower surface of the measuring part are 15 mm in thickness and 500 mm in width, and four Bakelite plates (2000 mm × 2, 1760 mm × 1,240 mm × 1) and six acrylic plates with a thickness of 15 mm, a width of 100 mm, and a length of 2000 mm, and the seams are shaped smoothly using clay. Details of the top of the measuring part (roof part) are shown in Figure 2-2. Nine acrylic sheets (2000 mm × 1, 1000 mm × 3, 335 mm × 1, 250 mm × 1, 150 mm × 2, 95 mm × 1) with a thickness of 10 mm and a width of 720 mm and different in length were installed. In order to make the cross section of the flow path even, the deflection preventing rib (10 mm × 30 mm × 720 mm) was attached at regular intervals, and the deflection preventing hook and the weight to which the load was applied were set in place. At the exit of the measuring part, the diffuser with an area ratio of 2.63 was provided to reduce the loss and to avoid disturbance.

1. The blower 2. The enlarged part
3. The collecting part 4. The throttle part
5. The measuring part 6. The diffuser

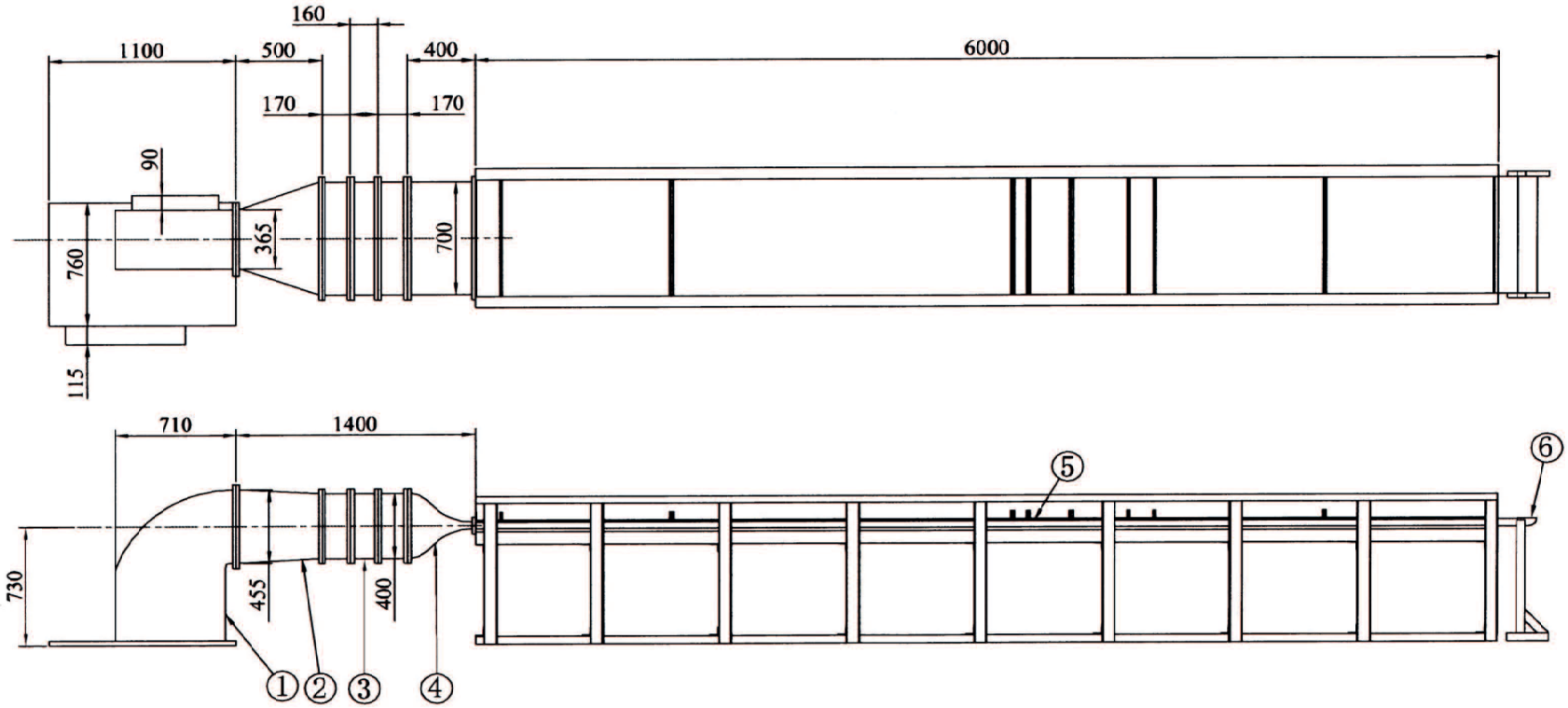

Fig.2-1 Two-dimensional turbulent channel

1. The top of the measuring part (roof part)
2. The rib

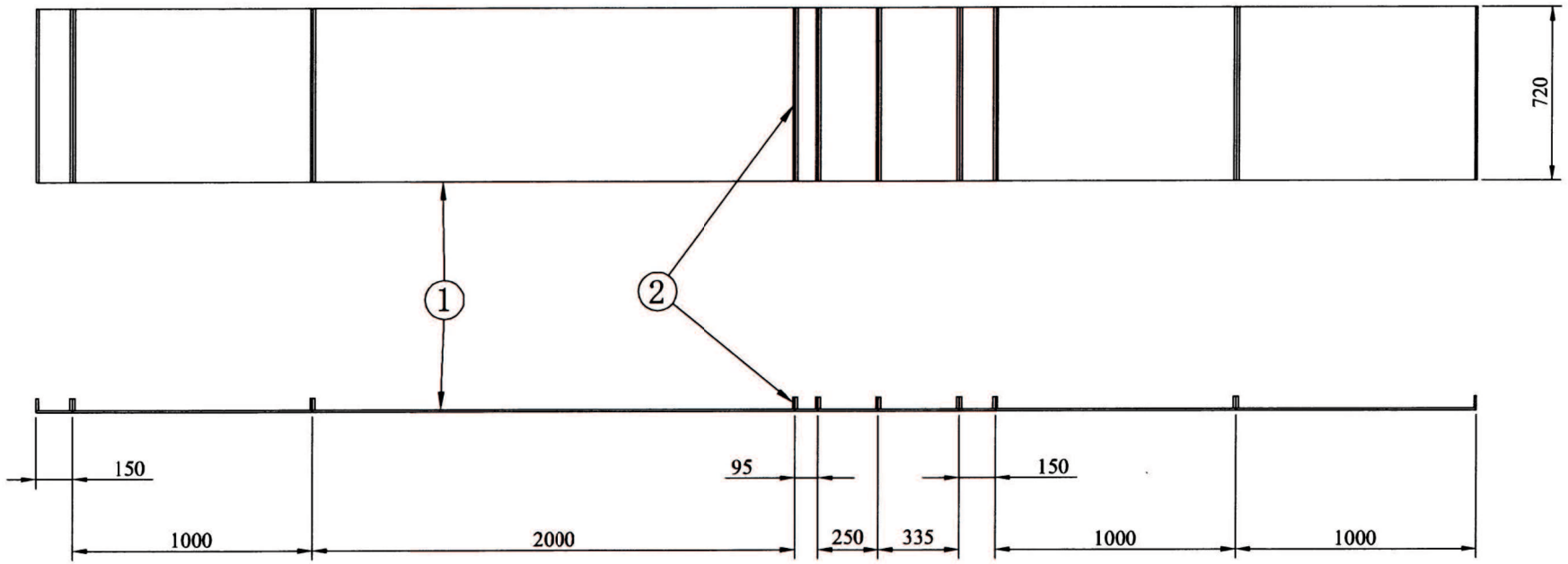

Fig.2-2 The main section of measuring part

2-2 The Differential Pressure Measurement

Differential pressure measurements were carried out to determine the tunnel free stream velocity by using pitot tubes, mean wall shear stress by using the sublayer plate, and the mean wall pressure by using the pressure hole on the surface.

Pito tube

Figure 2-3 shows the Pitot tube for calibration used for setting the cross-sectional center speed of this experiment. The manometer used in the experiment was a Gottingen type and was used to measure the flow velocity in the wind tunnel used together with the Pitot tube.

Tilt type manometer

An inclined manometer (SS type sharpness gradient pressure gauge manufactured by Shimadzu Corporation) was used to measure the wall static pressure and to measure the pressure difference occurring before and after the plate. Figure 2-4 shows the static pressure hole installed in plug. The inclination angle is set to 5.73°, and the head can be read by enlarging it about ten times. The minimum reading resolution is about 0.08 Pa. Ethyl alcohol (special grade 99.5%) was used as the liquid in the manometer.

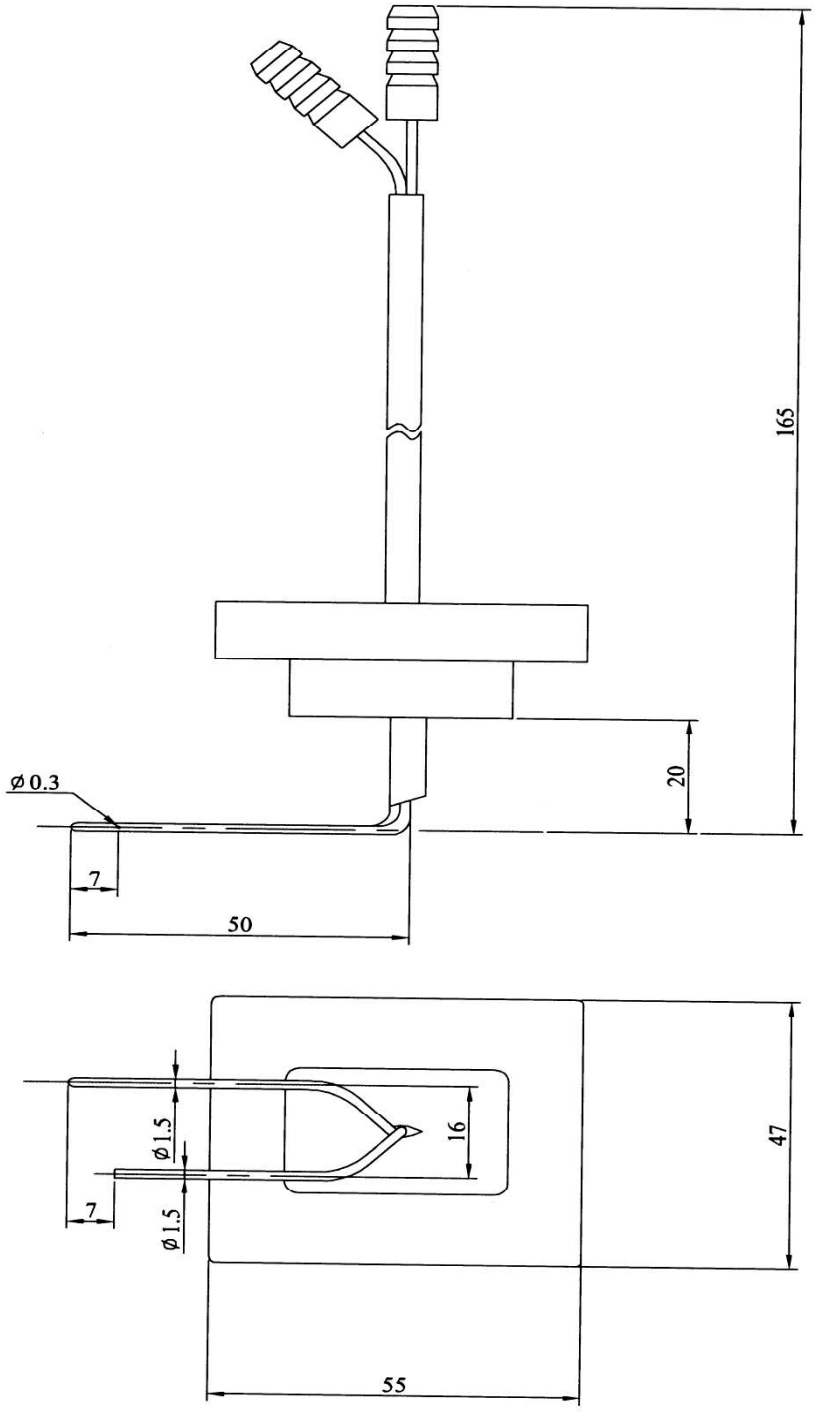

Fig.2-3 The setup of the Pitot tube

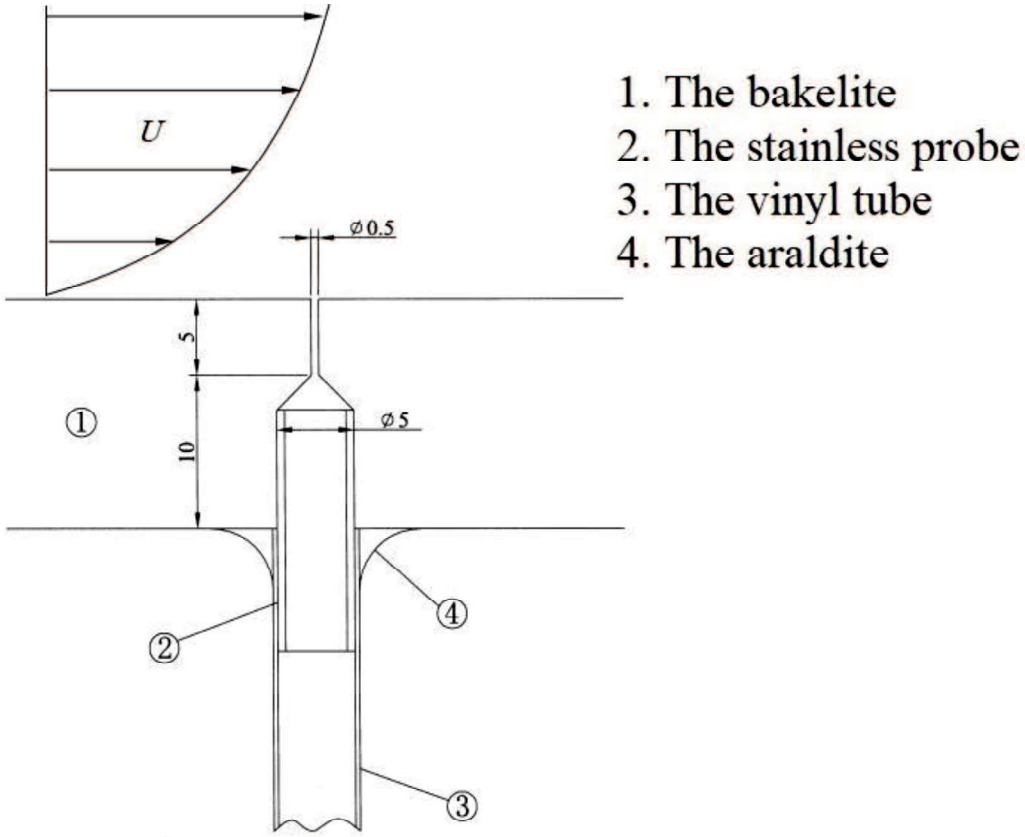

Fig. 2-4 The static pressure hole installed in plug

2-3 Velocity measurement

The I-probe used to determine the boundary layer characteristics was a hot wire sensor. A thin electrically heated wire is stretched between

prongs. The electrical resistance of the wire is related to its temperature. Depending on the velocity of the flow around the wire, heat is transferred to the flow, which tries to cool down the wire. The hot wire technique is a common technique for investigation in turbulent flows.

Hot-wire

For measuring the average flow velocity, a hot wire current meter system manufactured by Nippon Scientific Industry Co., Ltd. was used. The constant temperature type CTA 1010 is used for the hot wire current meter, and the frequency response is from D. C. to 22 KHz. The hot wire probe used for measuring the time average in the flow direction in this experiment is shown in Figure 2-5.

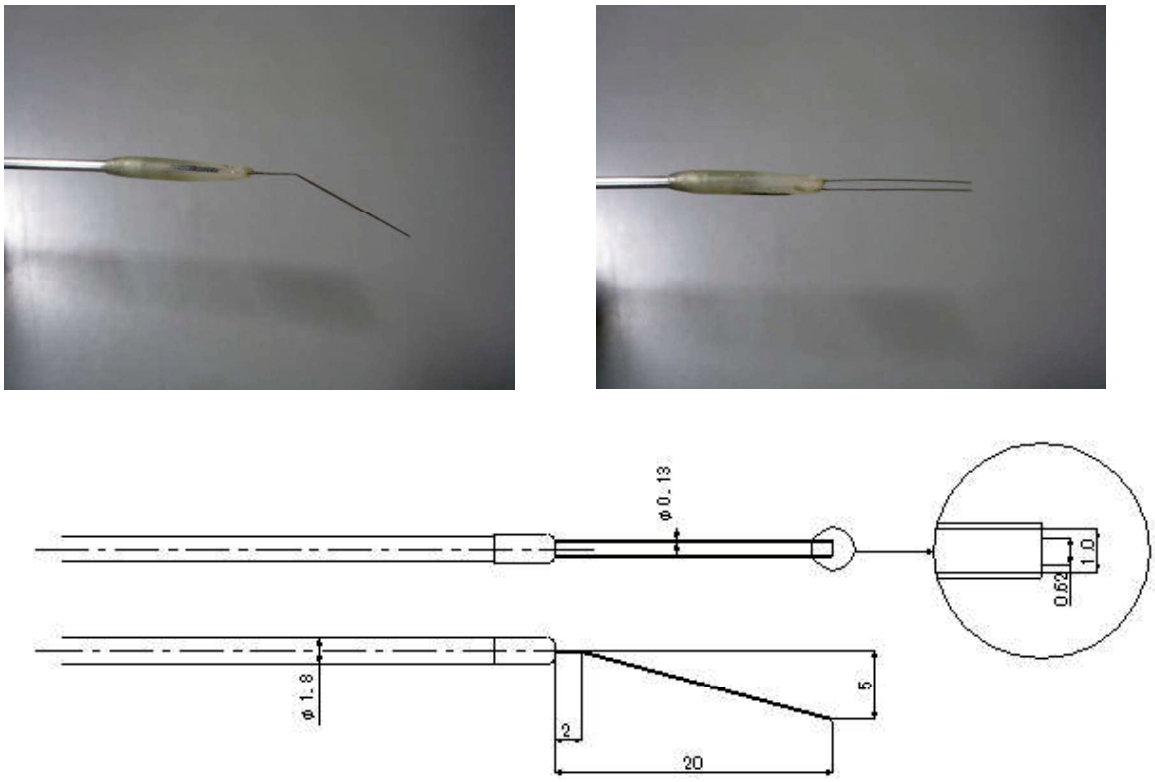

Fig.2-5 A hot wire measurement

At the front of the wire, a steel wire of φ 0.18 mm as a plunger is machined so that the front diameter is φ 0.13 mm and attached to the stem part with an epoxy adhesive. The distance between the tip of the probe is 1.0 mm, the distance from the tip of the stem to the tip of the prong is 20 mm, and in order to perform measurement near the wall surface, it is bent by 15^0. In addition, the hot wire sensor attached to the prong tip by the arc welding uses a tungsten wire with a diameter d = 3.1 μm, the copper is plated at both ends leaving a sensitive part of l_w = 0.62 mm. The aspect ratio of the perception part is l_w/ d = 200, the Reynolds number based on the main flow field and the length of the sensitive part is $u_\tau l_w/\nu$ = 22, and

the condition was agreed well with the securing sufficient spatial resolution by Ligrani. Further, the heating ratio of the hot wire was 1.5.

Data Acquisition System

For the measurement and analysis processing, a hot wire current meter, A / D converter (A / D 12-16 A made by CONTEC Co., Ltd., maximum output voltage 10 V), a personal computer, analog signals from the hot wire current meter which are converted by the AD converter were used in this experimental. The signal was converted into a digital signal, and calculation processing was performed in the personal computer. The sampling frequency at this time was set to 10 kHz, and the sampling time was set to 40 seconds.

Traverse device

To measure the section flow velocity by the hot wire current meter, a traverse device as shown in Figure 2-6 was used. A slide pack FBW5011R made by THK was installed in the lower part of the traverse device, and it is possible to move along the flow direction. It is possible to move along the spanwise direction by a shaft with φ25 mm, LM scale unit SC

(manufactured by THK). The motor is automatically fed in the vertical direction of the wall surface using a high torque 5-phase stepping motor (100 pulses / rotation). In addition, a height gauge (manufactured by Mitutoyo) SDV-15B reading accuracy 0.01 mm was installed to confirm the height in the vertical direction.

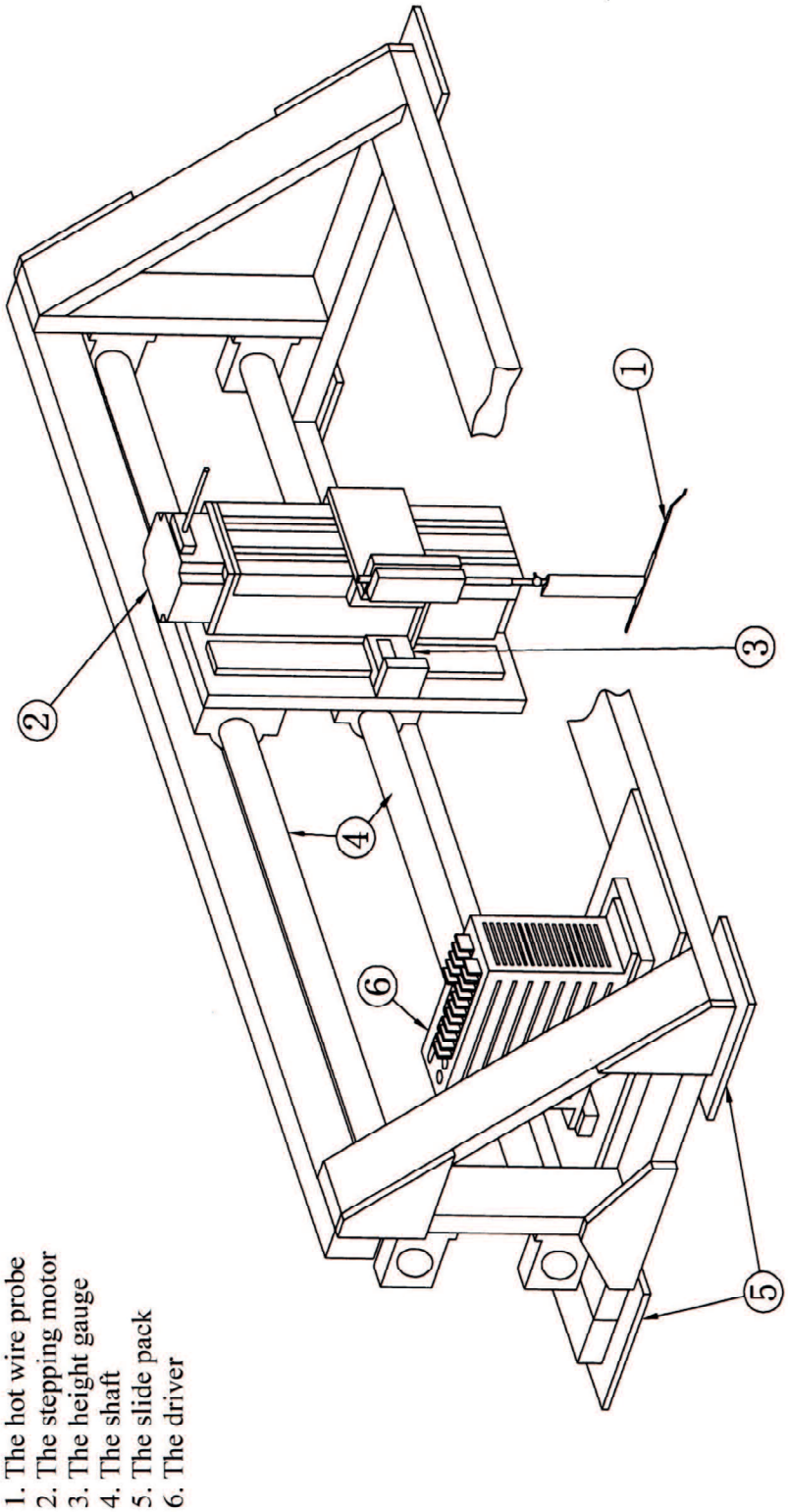

Fig.2-6 Traverse device for sensors

Chapter 3

Analytical Fundamentals

This chapter describes the theoretical background of the wall shear stress measurement with the sublayer plate.

3-1 Boundary layer

The layer moving next to a solid object placed in the wind tunnel, in which the velocity of the flow modifies from zero value for the surface of the object to the value corresponding to the outside flow and in which it occurs the intense manifestations of the friction forces is called the boundary layer (as show in Fig.3-1).

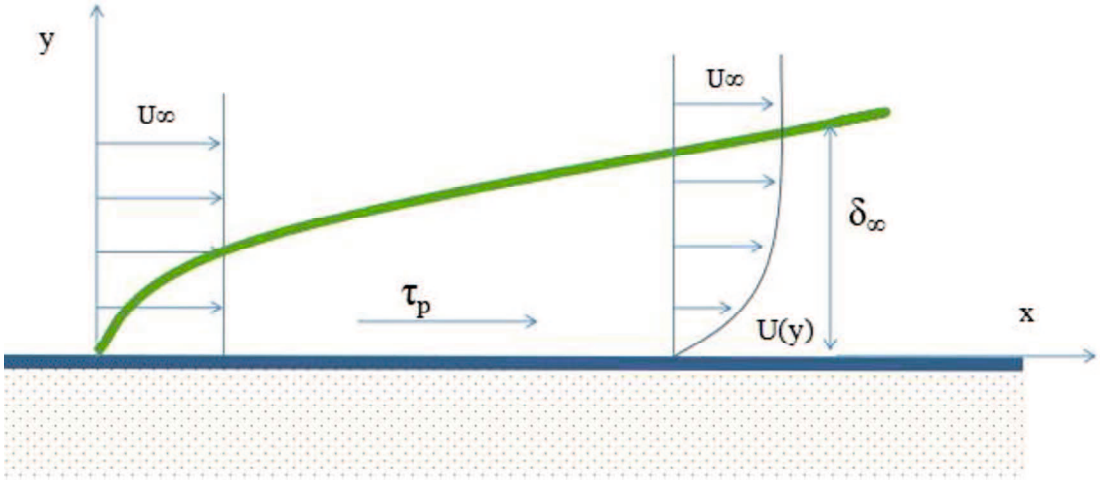

Fig.3-1 Boundary layer illustration

The concept of a boundary layer was introduced by Prandtl in 1904. He proposed that a flow around an object can be divided into two regions. One is a region where viscous effects are important, and another one is the remaining outer flow, which can be assumed to be inviscid. Boundary layer begins as a laminar flow with zero thickness at the leading edge of flat plate or finite thickness on a blunt object. After some distance, downstream, the laminar flow undergoes transition to turbulent flow. The simplest case of boundary layer study is the boundary layer developed on a flat plate, illustrated in figure 3-1. By comparison, the flow in the pipes and channels with a given pressure gradient, the main differences are:

1. The boundary layer develops continuously in the flow direction; its thickness, δ(x) increases with x;

2. the wall shear-stress variation, $\tau_p(x)$, is unknown;

In this layer, the suddenly increase of the tangential velocity determines great values for the velocity gradient and, as a consequence, the shear-stresses reach to considerable values, so the friction forces have great values, comparable with the inertial forces. Outside this boundary layer, the velocity gradient has a smaller value and the shear stress can be neglected, so the friction forces become negligible related to the inertial forces. The main characteristic of the boundary layer is its thickness, which is defined, conventionally, as being the distance δ from the body's surface, measured along the perpendicular to this surface, where the flow reaches around 99 % from the exterior potential flow velocity; it is estimated by relation 3.1.

$$\delta = y\Big|_{u=0.99U_\infty} \qquad 3.1$$

The main direction of the flow is along the x axis, with the velocity outside of the boundary layer, $u_0(x)$. Statistics fluctuate with y and is independent of z, so that the velocity depends both on x and y.

The boundary layer equation is obtain from the continuity equation and the Navier-Stokes equations system:

$$\frac{\partial u_x}{\partial x} + \frac{\partial u_y}{\partial y} = 0$$

$$\frac{\partial u_x}{\partial t} + u_x \frac{\partial u_x}{\partial x} + u_y \frac{\partial u_x}{\partial y} = -\frac{1}{\rho}\frac{\partial p}{\partial x} + \nu\left(\frac{\partial^2 u_x}{\partial y^2} + \frac{\partial^2 u_x}{\partial y^2}\right) \qquad 3.2$$

Considering the boundary layer thickness, δ, very small and making the approximation of the size for the equations terms, the system of equations 3.2, which characterize the flow in the boundary layer becomes:

$$\frac{\partial u_x}{\partial x} + \frac{\partial u_y}{\partial y} = 0$$

$$u_x \frac{\partial u_x}{\partial x} + u_y \frac{\partial u_x}{\partial y} = -\frac{1}{\rho}\frac{\partial p}{\partial x} + \nu \frac{\partial^2 u_x}{\partial y^2} \qquad 3.3$$

In turbulent flow, every flow parameter is considered to be made up of a temporal part and a fluctuating part:

$$U = U' + \overline{U} \qquad 3.4$$

where U' represents the fluctuating part of the velocity U and $\overline{U}$ represents the mean value of *U*.

Taking into account the relation 3.4 in the system of equations describing the flow in the boundary layer, equation 3.3, it is obtained the system of equations which characterize the boundary layer in a stationary flow, see equations 3.5.

$$\frac{\partial u_x}{\partial x}+\frac{\partial u_y}{\partial y}=0$$
$$\rho\frac{\partial u_x}{\partial t}+\rho u_x\frac{\partial u_x}{\partial x}+\rho u_y\frac{\partial u_x}{\partial y}=-\frac{\partial p}{\partial x}+\mu\nabla^2 u+\rho f_x \qquad 3.5$$

Assuming that:

- flow is steady: $u(t) = 0$,
- fluid is incompressible: $\rho = constant$,

there is obtained the momentum equation for the turbulent flow, see relation 3.6.

$$\rho\overline{u_x}\frac{\partial\overline{u_x}}{\partial x}+\rho\overline{u_y}\frac{\overline{u_x}}{\partial y}=-\frac{\partial p}{\partial x}+\mu\frac{\partial^2\overline{u_x}}{\partial y^2}-\rho\frac{\partial}{\partial y}(\overline{u_x'u_y'}) \qquad 3.6$$

As the fluid is considered a Newtonian one, Newton's relation regarding the wall shear stress is valid, see relation 3.7:

$$\tau=\mu\frac{u}{l} \qquad 3.7$$

where μ represents the dynamic viscosity, u is the flow characteristic velocity and l is the characteristic length of the flow. It can be seen that, in accordance with the boundary layer theory, and by considering u, the local velocity and y, the distance from the wall in the perpendicular direction to this wall, the wall shear stress is described by the relation 3.8.

$$\tau_w = \mu \frac{\partial u}{\partial y}\Big|_{y=0} \qquad 3.8$$

3-2 Turbulent Channel Flow

In the turbulent flows, the flow in the boundary layer is laminar for small distances and then it goes through a transition zone, for a specified critical velocity, reaching into a turbulent flow. In our experiments, A channel flow, through a rectangular duct of height H = 2h, length L_x =320h and aspect ratio W /H =17 is sketched in Figure 3-2.

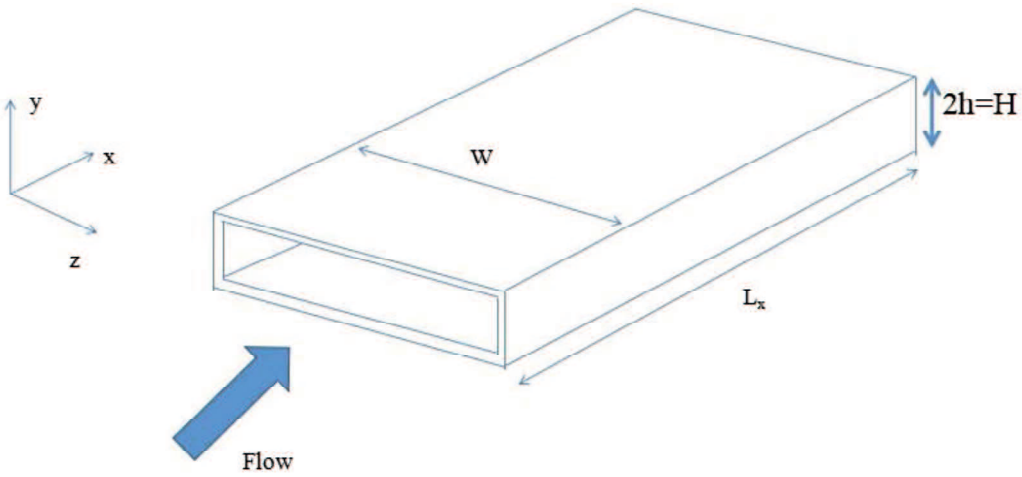

Fig.3-2 Sketch of a channel flow

The mean flow is predominantly in the x-direction, called streamwise, with the mean velocity varying mainly in the y-direction, called wall-normal direction. The extent of the channel in the spanwise direction

is large enough to consider the flow statistically homogeneous in the z-direction, called spanwise direction. The centerline is located at y = h and z = 0, while the bottom and the top walls are placed at y = 0 and y = 2h = H respectively. Far away from the inlet the flow in said to be fully developed and is statistically homogeneous in the x direction and statistically stationary. The layers of wall turbulence were defined in terms of y/h and $y^+ = y/\delta_\nu$. In the vicinity of the wall, where viscous effects dominate, viscous scales can be defined, based on the two locally important parameters ν and τ_x. These are:

$$u_\tau = \sqrt{\frac{\tau_x}{\rho}}, \quad \delta_\nu = \frac{\nu}{u_\tau}, \quad t_\nu = \frac{\nu}{u_\tau^2} \qquad 3.9$$

where u_τ , δ_ν and t_ν are a velocity, time, and space scale typical of the near-wall turbulence. An additional Reynolds number, the friction Reynolds number Reτ , characterize the near-wall turbulence and is defined as:

$$\mathrm{Re}_\tau = \frac{u_\tau}{\nu} h \qquad 3.10$$

The distance from the wall, measured in viscous lengths, also called wall units, is:

$$y^+ = \frac{y}{\delta_\nu} = \frac{y u_\tau}{\nu} \qquad 3.11$$

and is similar to a local Reynolds number, so that its magnitude can determine the relative importance of viscous and turbulent processes. According to the value of y^+, different regions, or layers, are defined.

The length of the inner layer depends on the range of the turbulence in the exterior flow, on the roughness of the surface and on the place of the flat plane in a configuration of contraction or diffuser. In this region, because the thickness of the layer is small enough, it can be assumed that the total friction is, approximate, equal with wall shear-stress. In the inner layer, the law of the wall is described by equation 3.12.

$$\frac{U}{u_\tau} = f\left(\frac{u_\tau y}{\nu}\right) \qquad 3.12$$

where f represents an universal function.

It can be remarked that the behavior of the velocity near the wall is independent on the conditions of the flow far from the wall. The inner layer corresponds roughly to: $y/\delta < 0.1$.

In the viscous layer $y^+ < 50$, the viscosity has a direct effect on the shear stresses. In the inner layer $y/h < 0.1$ the velocity is assumed not to be a function of the position y/h across the channel but on the distance y^+ from the wall. Within the viscous sublayer, in the innermost edge of the inner

layer, from the definition of u_τ leads to: $U^+ = y^+$. At sufficiently high Reynolds numbers, a region between the outermost part of the inner layer $y^+ > 30$ and the innermost part of the outer layer exists $y/h < 0.3$, where the following logarithmic law, or simply log law, holds:

$$U^+ = \frac{1}{\kappa} \ln y^+ + B \qquad 3.13$$

where $\kappa = 0.41$ is the von Kármán constant and $B \approx 5.2$. Both are deemed to be universally constant at high Reynolds numbers. In this region, takes place a suddenly increase of the boundary layer thickness, δ, and a suddenly change of the velocity; the velocities increase very fast near the wall and they have the tendency to become uniform along the normal to the wall.

With similar arguments, the velocity can be assumed to be a function of y/h only close to the centerline of the channel, where the viscous effects are negligible. In this region, the following velocity-defect law can be derived:

$$U^+ = -\frac{1}{\kappa} \ln y^+ + B_1 \qquad 3.14$$

where the constant B_1 is flow-dependent. The constant B_1 is normally nonzero, but is relatively small, meaning that the Equation 3.14 is a good approximation of the defect-velocity profile at the centerline.

In the outer layer $y^+ > 50$ the effect of viscosity is negligible. In this region the velocity law is complex. It is called the overdrawn speed law; it is difficult to provide, from the theoretical point of view, the velocity distribution. The turbulent zone concerns the other 85 to 95% from the boundary layer thickness. Due to its complexity and difficulty, this region cannot be used for the experimental evaluation of the wall shear stress, for the studied case.

3-3 Friction law

The wall shear stress normalized by a reference velocity is called a skin friction coefficient. On the basis of Uc skin-friction coefficients can be defined:

$$C_f = {}^{2\tau_w}\!\!\diagup\!\!_{(\rho U_c^2)} \qquad 3.15$$

which is function of the Reynolds number only. *U*c is the centerline velocity. In laboratory experiments, C_f is a mild function of the aspect ratio of the channel, as the flow uniformity across the channel decreases for decreasing aspect ratios.

Taking the examination volume in the turbulent development region of the two-dimensional channel flow and setting the equilibrium formula of the force, it can be expressed as follows.

$$-\tau_w \Delta L S = pA - (p + \Delta p)A \qquad 3.16$$

S is open veranda length (= 2 (H + W)), and A is the cross-sectional area (=HW). Here, when $\Delta p = dp$, $\Delta L = dx$, $W >> H$, the wall shear stress τ_w is:

$$\tau_w = -\frac{dp}{dx} \times H \qquad 3.17$$

The wall frictional resistance coefficient C_f is equation 3.15. So C_f would be:

$$C_f = -\frac{dp}{dx} \times \frac{2H}{\rho U_c^2} \qquad 3.18$$

Here, the pressure coefficient C_p is:

$$C_p = \frac{2p}{\rho U_c^2} \qquad 3.19$$

Therefore,

$$C_f = -\frac{dC_p}{dx} \times H \qquad 3.20$$

The law of the wall can be used to determine the Reynolds number dependence of the skin-friction coefficient and eventually predict its value.

3-4 Boundary shear stress

The wall shear stress of the channel flow was determined as the mean of the values obtained from the velocity gradient near the wall and from the pressure gradient. Considering the previous analysis, the sublayer plate is based on the similarity law of the viscous sublayer

$$U^+ = y^+, \quad U^+ = \frac{U}{u_\tau}, \quad y^+ = \frac{u_\tau y}{\nu}$$

The measured differential pressure of the sublayer plate is correlated to the local wall shear stress assuming a relationship between this pressure and the velocity distribution close to the wall. This correlation is determined empirically and usually formulated as a calibration curve of the type:

$$h^+ = f(\Delta p^+), \quad h^+ = \frac{\tau_w h^2}{\rho \nu^2}, \quad \Delta p^+ = \frac{\Delta p h^2}{\rho \nu^2}$$

where f represents a universal function.

Chapter 4

Flow Field and Sublayer Plate

4-1 Flow field

Figure 4-1 shows a schematic diagram of the flow field and the coordinate system of the channel, the dimensions of which are 700 mm (width) 40 mm (height) 6,000 mm (length). The Reynolds number based on the channel center velocity and height Re = U_CH/v was varied from 8,000 to 24,000. The local wall shear stress was determined based on the streamwise gradient of the wall static pressure for the fully developed equilibrium state sufficiently far from the channel entrance. Figure 4-2 shows that pressure coefficient C_p of wall static pressure is shown against x/H. From the figure, C_p linearly descends with x/H = 56, indicating that the flow field is the fully developed situation. Figure 4-3 shows the variation of the local skin-friction coefficient as a function of Reynolds number. The experimental results agreed well with the semi-empirical equation proposed by Dean based on a survey of available experimental data (Dean, 1978). This agreement appears to be good at higher Reynolds

numbers. The result yielded a skin friction coefficient based on the pressure gradient at the surface.

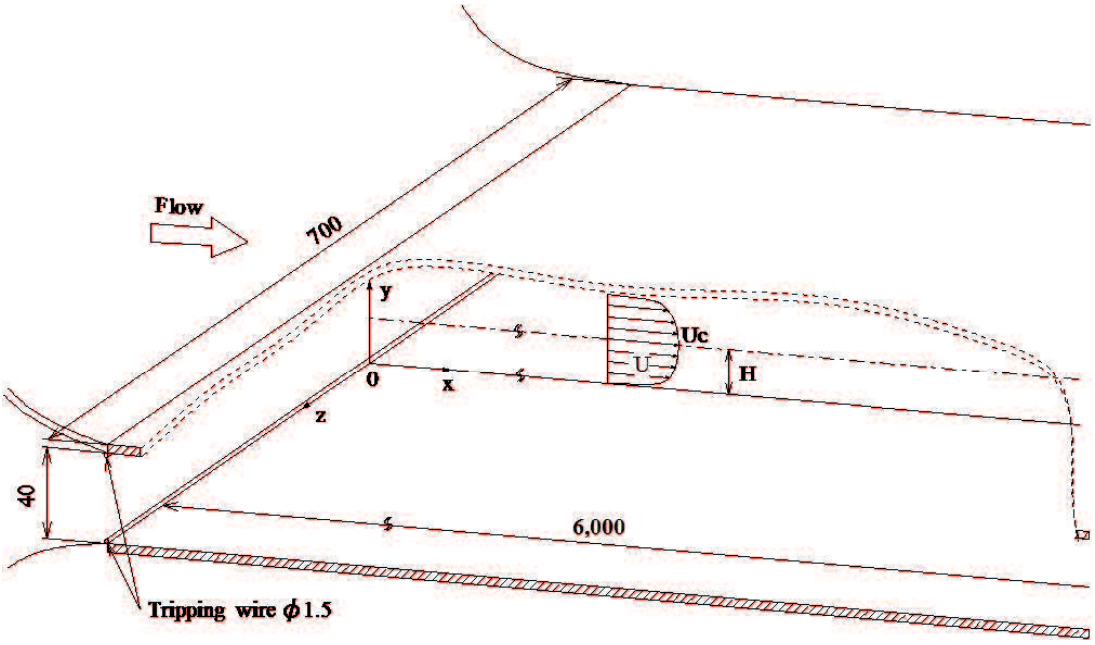

Fig.4-1 Schematic diagram of the flow field and the coordinate system of the channel

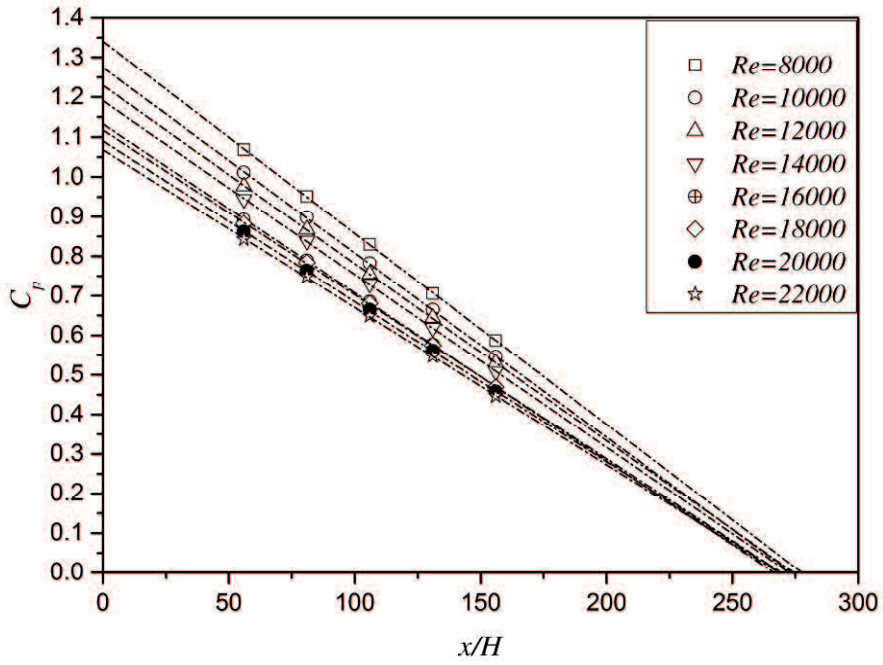

Fig.4-2 Pressure coefficient C_p of wall static pressure

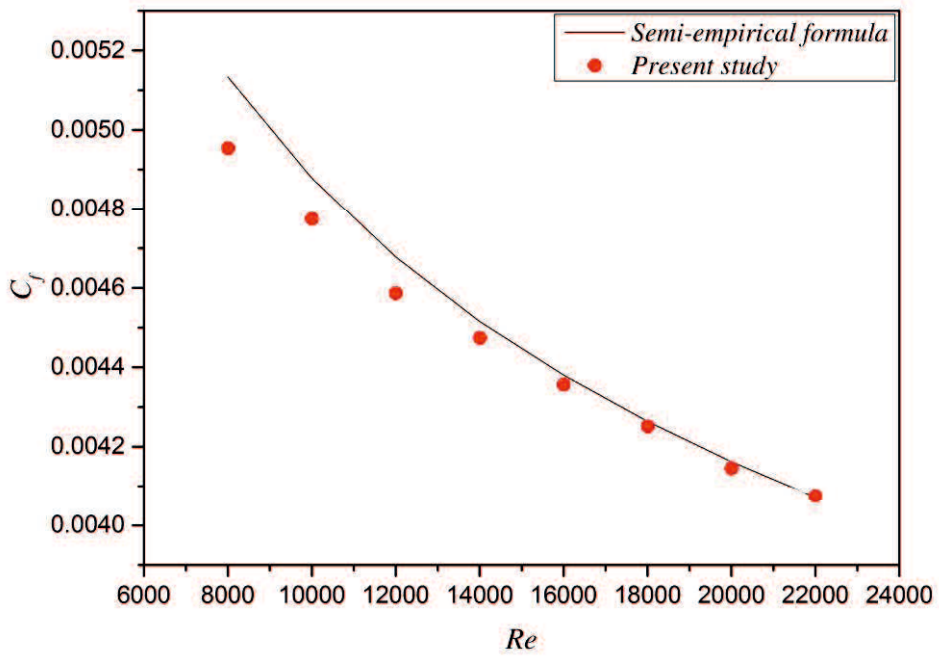

Fig.4-3 Variation of the local skin-friction coefficient as a function of Reynolds number. A semi-empirical formula was calculated by Dean. The integration of Dean's formula provides good agreement with all parameters and coincides with the 'optimum log-law' for skin friction.

Figure 4-4 shows that the difference between the data obtained in the present study and Dean's data. Dean's equation provides a reliable method for the calculation of the friction coefficient and for the mean velocity distribution over a wide range of Reynolds numbers. For high Reynolds numbers, the percentage error is less than 2%. However, for

lower Reynolds numbers, especially at Re = 8,000, the aspect ratio, which is defined as W/H, might be affected by the non-uniform shear stress around the corners of the plate on the friction law. In the discussion on the magnitude of the Karman constant (Nagib and Chauhan, 2008), the uncertainty in the wall shear stress measurements must be less than 2%. Thus, the experimental results for Re = 8,000 should be disregarded.

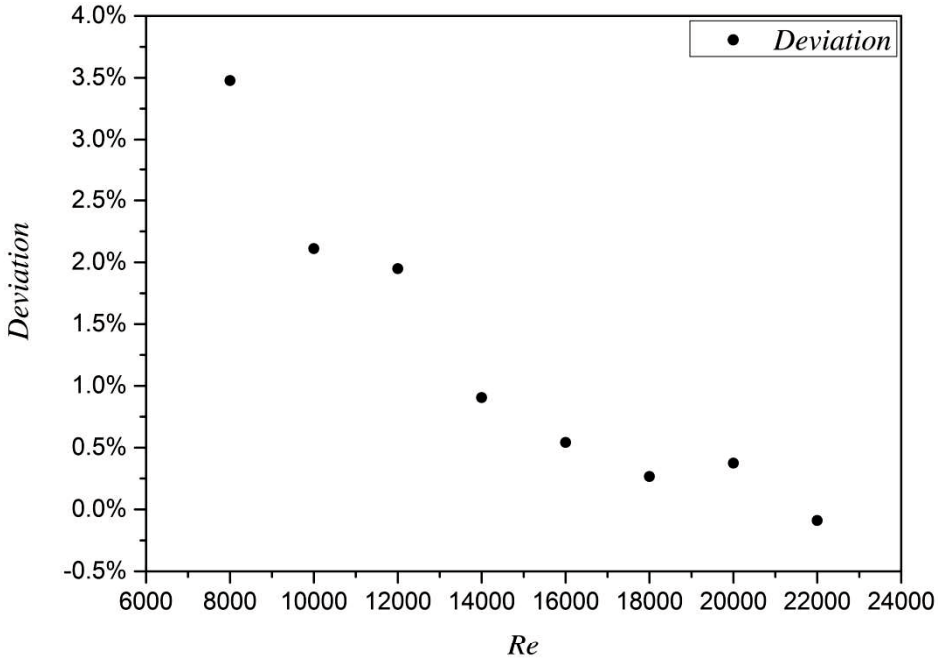

Fig.4-4 the difference between the data obtained in the present study and Dean's data

The logarithmic velocity profiles at downstream positions after a streamwise distance equal to 81 times the channel height (x = 3,240 mm) as measured from the entrance are given in Fig. 4-5. We used a microscope with an accuracy of ±0.005 mm to determine the hot-wire

probe origin. Figure 4-5 shows the comparison of the velocity profile in the present channel flow and the log-law. There are many arguments on the standard values involved in the logarithmic law (see e.g. Nagib and Chauhan, 2008). For the wall layer expected by the presence of the logarithmic velocity profile in the layer greater than y^+=100, the velocity profile well agrees with the standard log-law. The flow field used in the present experiments is relatively low. The logarithmic velocity profile seems to appear for the narrow layer in Fig.4-5. The experimental data show that the present flow field contains the sublayer covered by the wall layer. These experimental facts give guarantees that the present channel flow is suitable one for calibration of the local wall shear stress device. Although the universal value of the Karman constant for a two-dimensional channel flow remains unknown, the experimental data of the present study agree well with the solid line representing the results of a survey conducted by Nagib and Chauhan (2008).

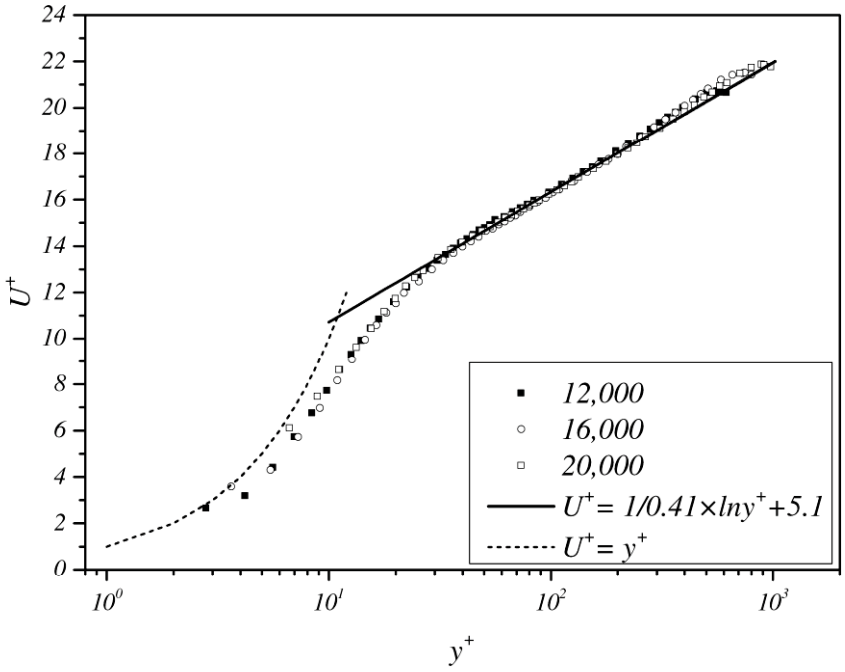

Fig.4-5 Log-law profiles at Reynolds numbers of 12,000 (■), 16,000 (○), and 20,000 (□). The solid line indicates the log-law profile, and the dashed line indicates the law of the wall in the viscous linear sublayer.

The streamwise turbulent intensity profiles are compared to the experimental data at low Reynolds numbers reported by Wei and Willmarth (1989) and Antonia et al. (1992) in Fig. 4-6. The maximum value of the turbulent intensity is in reasonably good agreement with their experimental data. The measured streamwise mean and turbulent velocities are obtained using a single hot-wire probe and a constant-temperature anemometer. The hot-wire measurement is

performed using a tungsten-filament sensor having a diameter of 2.5 μm and an active length of 0.5 mm. The active length is less than 20 times the viscous wall unit, that is, spatial resolution of the hot-wire sensor is satisfied for turbulence measurement (Ligrani and Bradshaw, 1987).

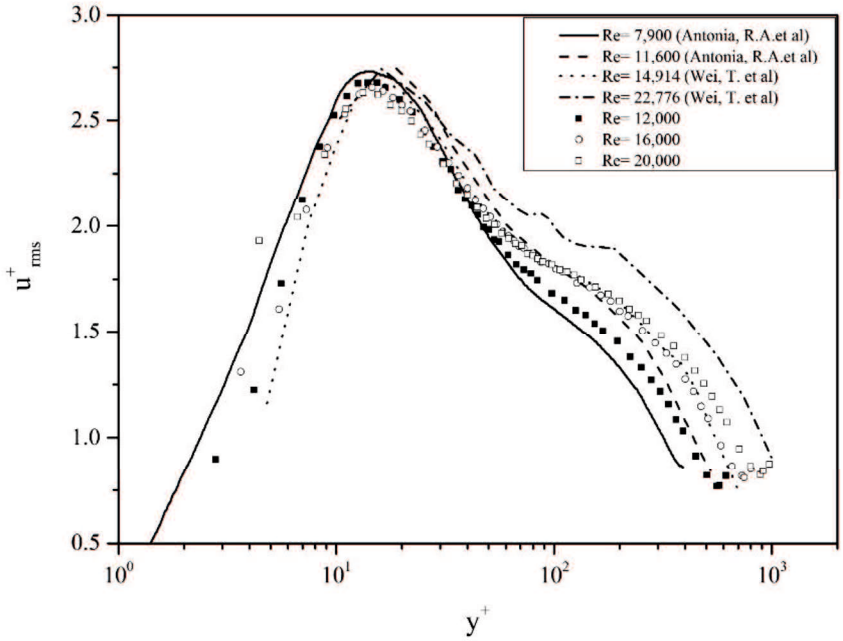

Fig. 4-6 Experimental and numerical streamwise turbulent intensity profiles obtained in previous channel flow experiments and in the present study at Reynolds numbers of 12,000 (■), 16,000 (○), and 20,000 (□). The solid and dashed lines indicate the streamwise turbulent intensity profiles calculated by Antonia et al., and the dotted and dash-dotted lines indicate the streamwise turbulent intensity profiles obtained by Wei and Willmarth(1989).

4-2 Sublayer plate

4-2-1 Rectangular sublayer plate

The sublayer plate is a simple, thin, rectangular plate attached to the wall, as shown in Fig. 4-7. The sublayer plate method is an indirect technique for the measurement of wall shear stress. In this method, a small obstacle is placed on the wall surface, and the difference in pressure is measured and interpreted as shear stress by means of a calibration under known shear stress conditions. The obstacle in the plug is a thin, rectangular plate. And the plug was installed tight with the test wall surface. The protrusion of the plate into the flow (its height above the test surface) was designed as the thickness of the plate. The thickness of the sublayer plate, h, ranges from 0.1 to 0.3 mm. For the channel flow of the present study, these thicknesses correspond to 2.3 to 14.5 times the viscous wall unit. Plates having an aspect ratio, w/l, of 3 for streamwise plate lengths, l, of 5 and 10 mm were used to investigate the angular resolution in chapter 5. The thin plate is made of phosphor bronze and was cut by electric discharge machining. In order to investigate stagnation at the leading edge and separation at the trailing edge, pressure measurements were conducted using pressure taps of 0.3 mm in diameter situated close to the plate edges. The measured pressure is probably influenced by the relative position of

the pressure tap with respect to the plate edge and the open area of the pressure tap. The differential pressure was obtained using a tilt-type manometer. The resolution of the differential pressure was 0.08 Pa. The pressure is slightly reduced if the open area is too small or too large. Some results of the preliminary experiment on the pressure measurement in terms of the gap, Δx, are presented and discussed in chapter 5. The open area of the pressure taps should be independent of the separation and reattachment on the wall. Half of the static pressure tap diameter, $\Delta x = 0.15$ mm, is used as the overlap length in most of the experiments.

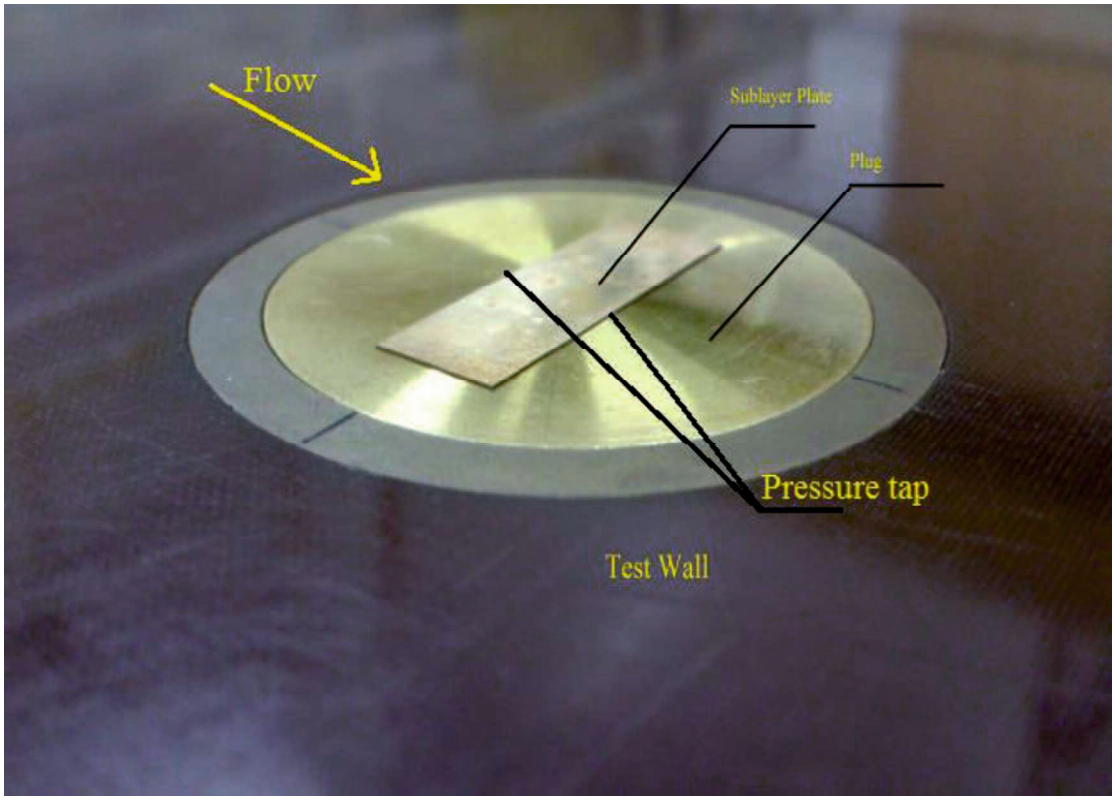

Fig. 4-7 Photograph of sublayer plate installed in test wall. A bronze plug has 2 small static pressure taps and a rectangular shaped

phosphor bronze plate located on the plug. The longer edges of the plate adjusted to the pressure taps

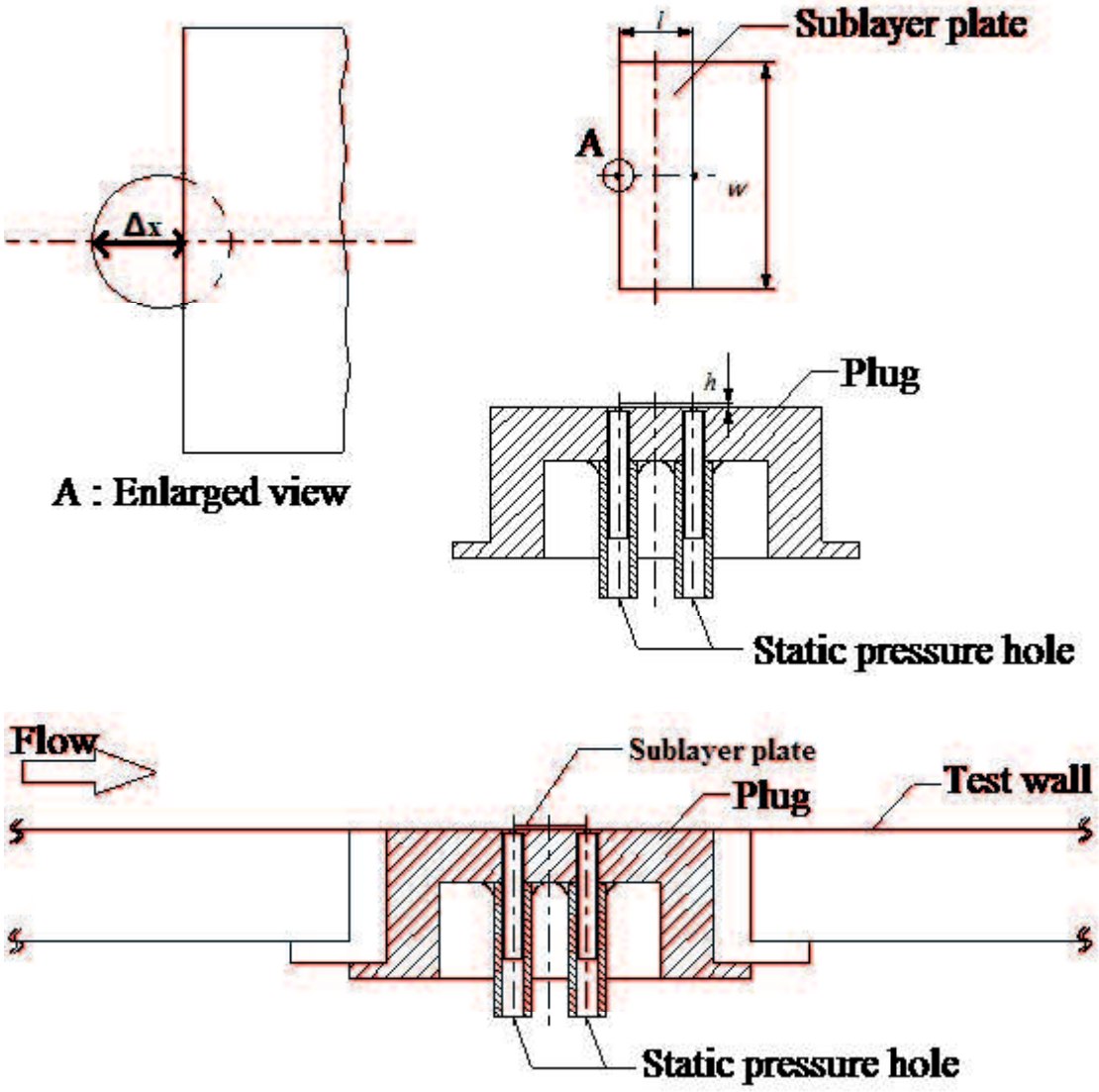

Fig.4-8 Schematic diagrams of the rectangular sublayer plate (Δx: diameter of the gap, h: height of the plate)

4-2-2 Circular sublayer plate

The circular sublayer plate was a simple, circular, thin plate that is attached to the wall, as shown in Fig. 4-9. The thickness of the plate, h, ranged from 0.1 to 0.3 mm. For the channel flow in the present study, these thicknesses correspond to 2.4 to 14.8 times the viscous wall unit. The diameter of the plate, D, was 5 mm or 10 mm. The circular plate was made of phosphor bronze and was fashioned by electric discharge machining. The diameters of the plate were in the range of 120 to 500 viscous wall units. In order to investigate stagnation at the leading edge and separation at the trailing edge, pressure measurements were conducted using pressure taps with diameters of 0.3 mm situated close to the plate edge. The circular sublayer plate designed for wall shear stress vector measurement had static pressure taps at 45° increments around it edge. The measured pressure is influenced by the relative position of the pressure tap with respect to the plate edge and the open area of the pressure tap. The differential pressure was obtained using a tilt-type manometer. The open area of the pressure taps should be independent of the separation and reattachment on the wall. Half of the static pressure tap diameter, Δx = 0.15 mm, was used as the overlap length in the following experiment.

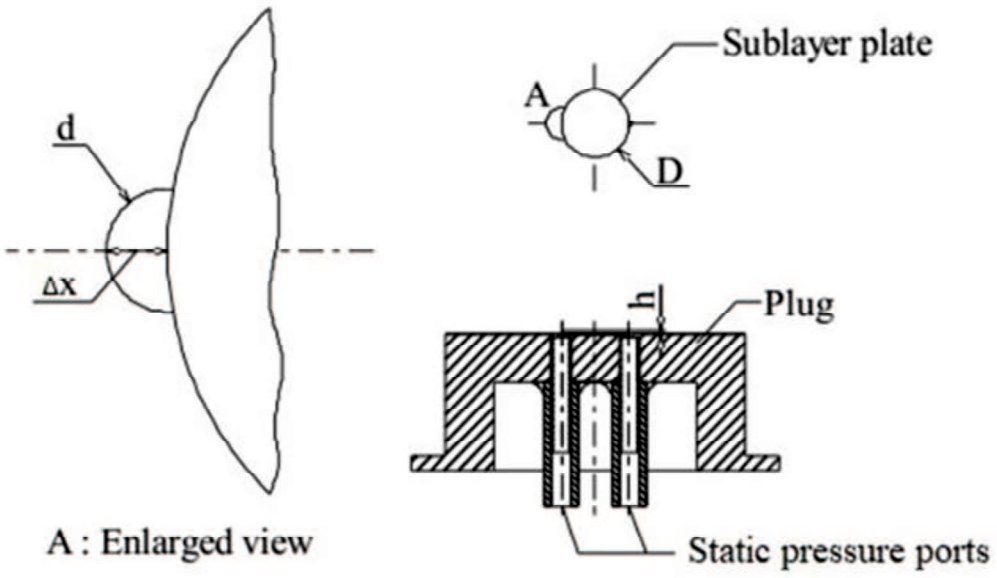

Fig.4-9 Schematic diagrams of the circular sublayer plate (D: diameter of the circular plate, d: diameter of the pressure tap, Δx: diameter of the gap, h: height of the circular plate).

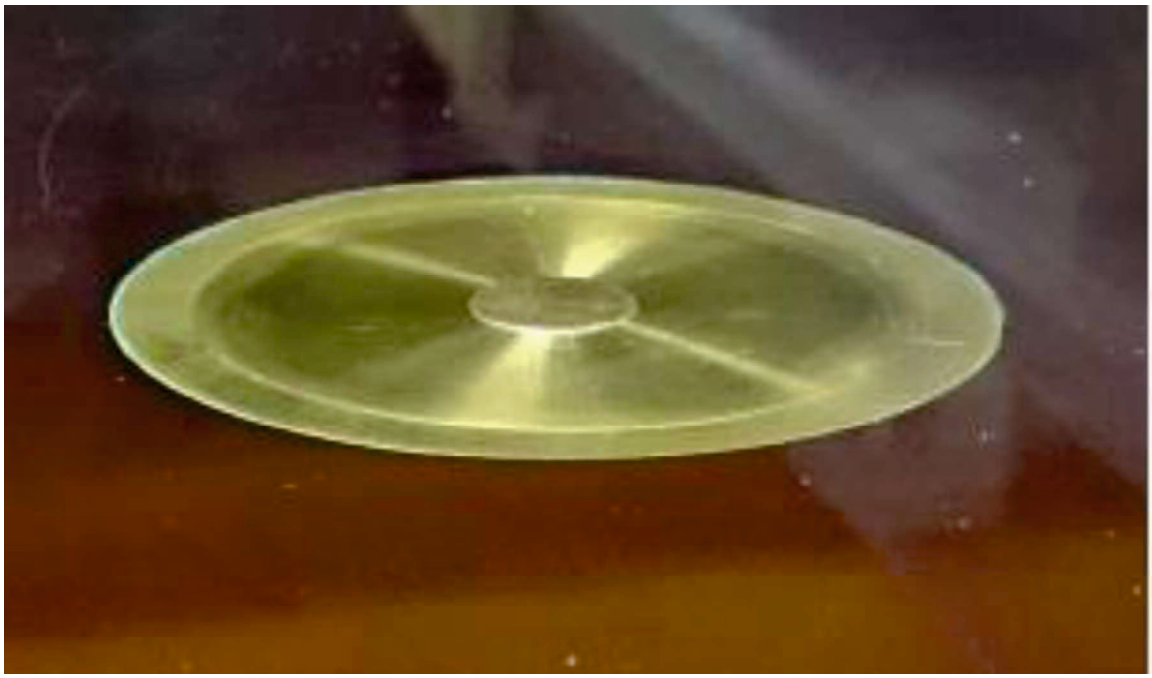

Fig. 4-10 Photograph of circular sublayer plate installed in test wall

Chapter 5

Sublayer Plate Measurement

5-1 Rectangular plate

At first, we want to propose the measurement procedure of sublayer plate using rectangular sublayer plate. Once the rectangular sublayer plate is calibrated, the following procedure can be used for a measurement within three-dimensional boundary layer: first, the sublayer plate is placed on the test wall surface (as shown in Fig. 4-7). The pressure difference ΔP is recorded (as shown in Fig.5-1). The direction of wall shear stress α, is determined from Fig. 5-8. Finally, from Fig.5-2, the magnitude of the wall shear stress is determined.

The sublayer plate is easier to build than the sublayer fence and requires only a precise manometer to read the pressure difference, ΔP, between upstream and downstream of the plate. In order to obtain the calibration curve, the correlation between the pressure difference and the wall shear stress was examined for a plate placed on the wall in the channel flow at a streamwise distance of 81 times the channel height from the entrance. The thickness of the plate was on the same order as the diameter of the static taps in the wall, and separation bubbles were likely to appear in

front of and behind the plate. The pressure difference presumably depends on the relative positioning of the plate with respect to the taps. The influence of the relative positioning on the wall pressure measurements was investigated using plates of three thicknesses, namely, $h = 0.1$, 0.2, and 0.3 mm, and the measured static wall pressure is plotted in Fig. 5-1.

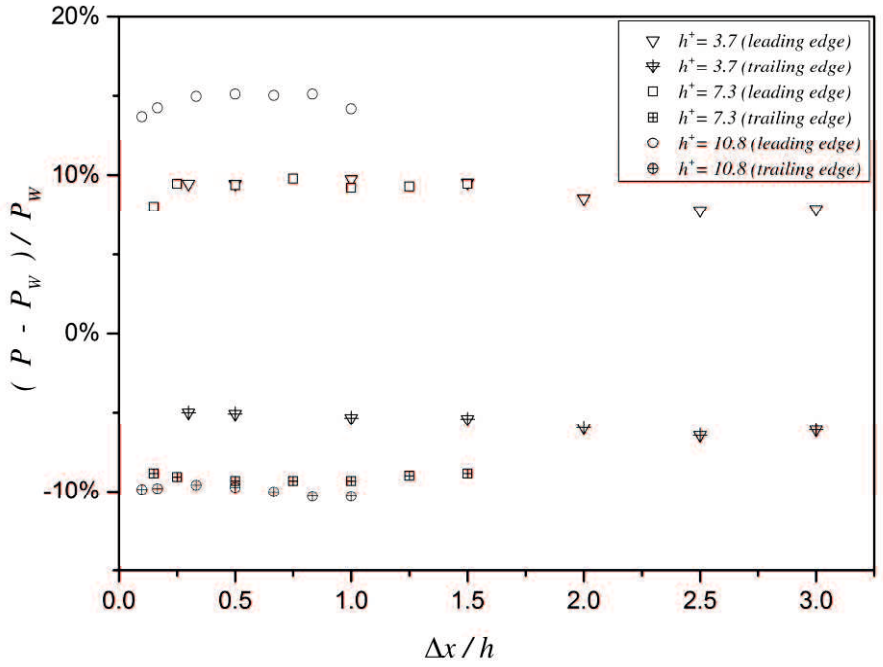

Fig. 5-1 Static pressure at the leading and trailing edges of the plate as a function of the gap between the plate and the pressure tap.

In the figure, P is the pressure with the sublayer plate, and P_w is the wall static pressure without the sublayer plate at the same location. Of course, because the pressure and the wall static pressure are not measured at the same time, flow conditions must remain the same for the pressure difference to be valid. The experiments were conducted at Re = 16,000,

and l was fixed at 10 mm. The plate thicknesses correspond to 3.7, 7.3, and 10.8 times the viscous wall unit for h = 0.1, 0.2, and 0.3 mm, respectively. The stagnation pressure at the leading edge of the plate was relatively high for the thickest plate (h^+ = 10.8), where the leading edge was located in the buffer layer. At the trailing edge, the magnitude of the negative pressure for the thinnest plate (h^+ = 3.7) was smaller than in the other cases. The thinnest plate was enveloped by a linear sublayer, and the viscous effect appeared to prevent the occurrence of a larger negative pressure at the trailing-edge-facing step. The heights of the protrusions on the wall were classified as being fluid-dynamically smooth if the protrusion height was less than five times the viscous wall unit (see, e.g., Schlichting, 1979). Based on the experimental results for the cases of h^+ = 7.3 and 10.8, the positive pressure at the leading edge and the negative pressure at the trailing edge are approximately independent of the gap, Δx, over the range of 0.15 ± 0.05 mm. The static pressure tap should be located in the separation bubble near the leading and trailing edges. In other words, the pressure taps should not be located near the separation and reattachment points on the wall. Otherwise, the relative distance between the tap and the plate edge should not be too small, because the static pressure measured through a small tap is influenced by viscosity.

Calibration curves must be determined as the functional relation between two dimensionless quantities derived from dimensional arguments, in a manner similar to that for a Preston tube or a sublayer fence, as follows:

$$\mathrm{Y}^* = \log(\tau_w h^2 / \rho\nu^2) \quad \text{and} \quad \mathrm{X}^* = \log(\Delta P h^2 / \rho\nu^2) \qquad 5.1$$

The functional relation between the two dimensionless quantities for three plate thicknesses (h = 0.1, 0.2, and 0.3 mm) is plotted for l = 2, 5 and 10 mm in Fig. 9. The straight line indicates the relation obtained by the least-squares method for all of the experimental data obtained with sublayer plates of nine sizes for l = 2, 5 and 10 mm. All of the experimental results can be well represented by a universal calibration curve calculated by the following equation without any clear differences associated with the thickness and length of the plate:

$$\mathrm{Y}^* = 0.771X^* - 0.615 \qquad 1.72 < \mathrm{X}^* < 3.90 \qquad 5.2$$

In the previous experiment (Mochizuki, et al., 2014), the experimental data was obtained for three thicknesses and l = 10 mm. As shown in Fig. 5-2, for 1.72 < X* < 2.45 and $h^+ < 5$, the data in the previous and present experiments well agrees with the solid line plotted by Equation 5.2. Compared to the calibration curve obtained by the sublayer fence (Higuchi, 1985) (in the viscous sublayer), the pressure difference

normalized by the wall variables obtained from the streamwise pressure

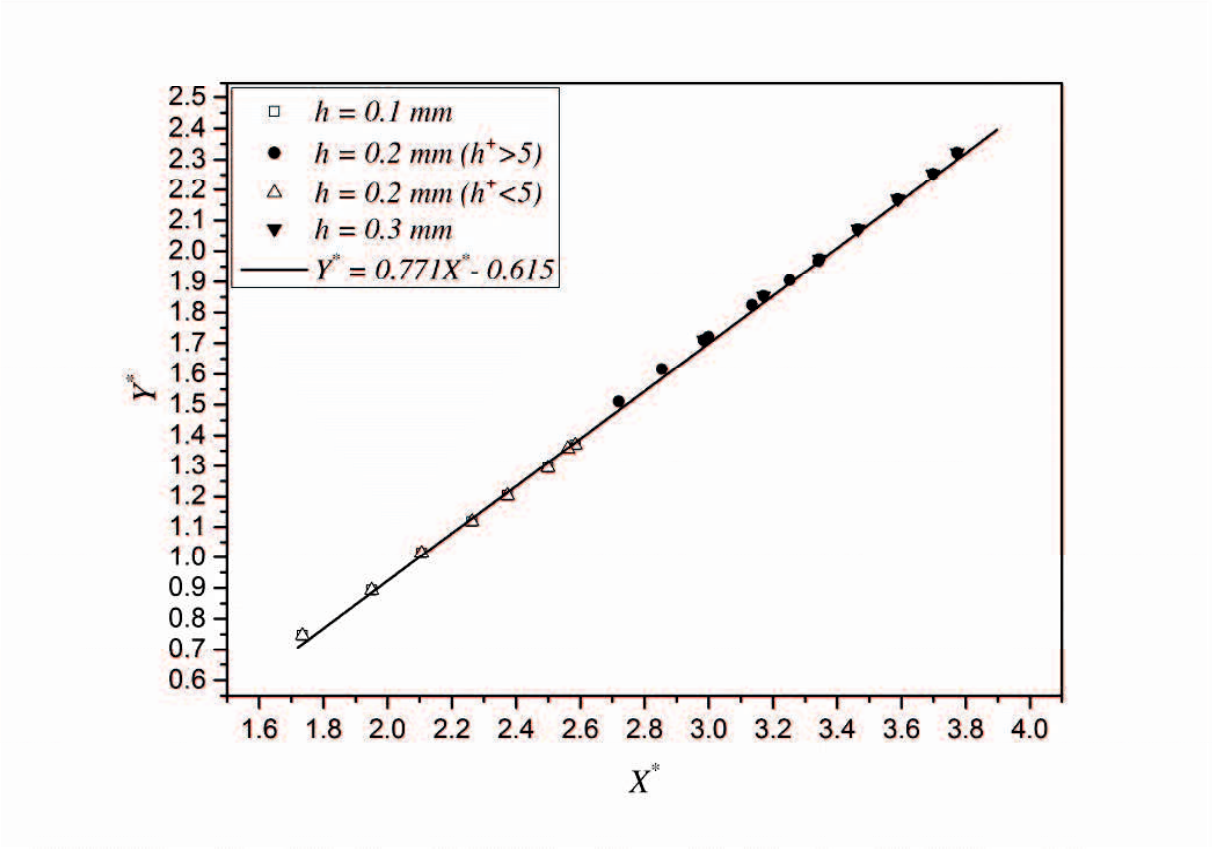

(a) l = 2 mm

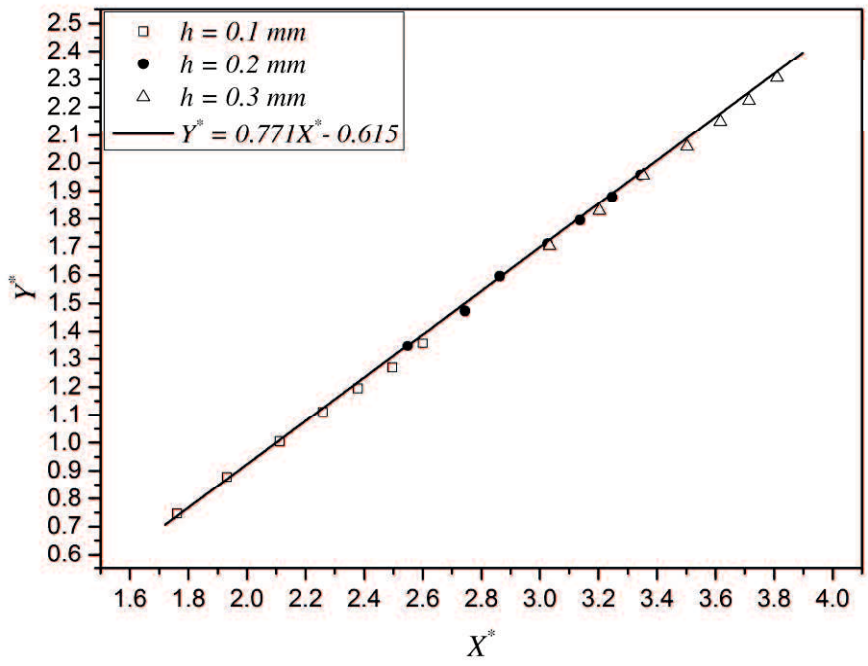

(b) *l = 5 mm*

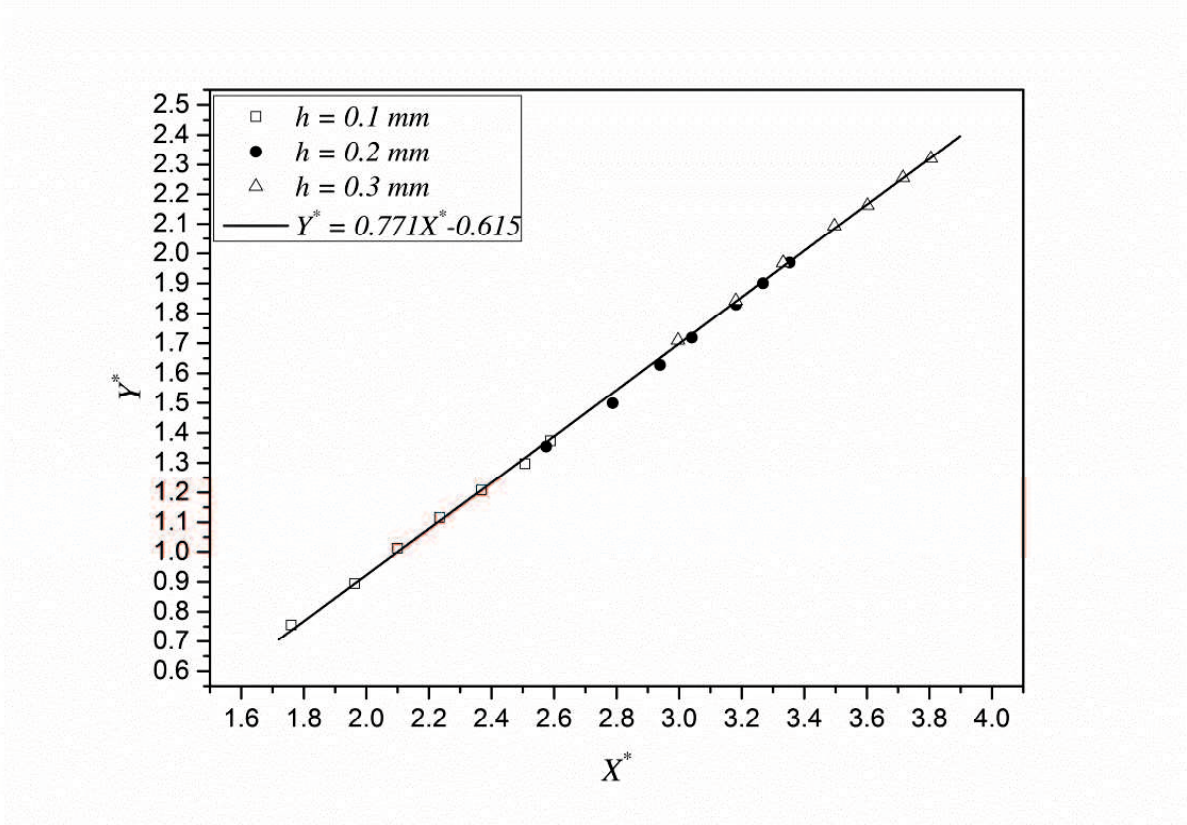

(c) *l = 10 mm*

Fig. 5-2 Calibration curve for three parameters obtained from experimental data.

Figure 5-3 shows the deviation between the calibration curve and the data obtained in the present study. The maximum deviation between the calibration curve and the data obtained in the present study is less than 1%. Moreover, X* ranges from 1.72 to 3.90. Figure 5-3 indicates that as X* increases, the range of deviations increases. The curve trend is the most gentle for l = 2 mm. The deviation is the smallest for l = 10 mm. Although it might appear that the sublayer plate cannot be used to measure the local wall shear stress and has low spatial resolution, the Preston tube requires a

longer longitudinal tube length equivalent to 10 times the tube diameter, as well as spanwise separation from the wall static tap. In most flow fields encountered in engineering, 100 times the viscous wall unit is less than 1/100 the boundary layer thickness.

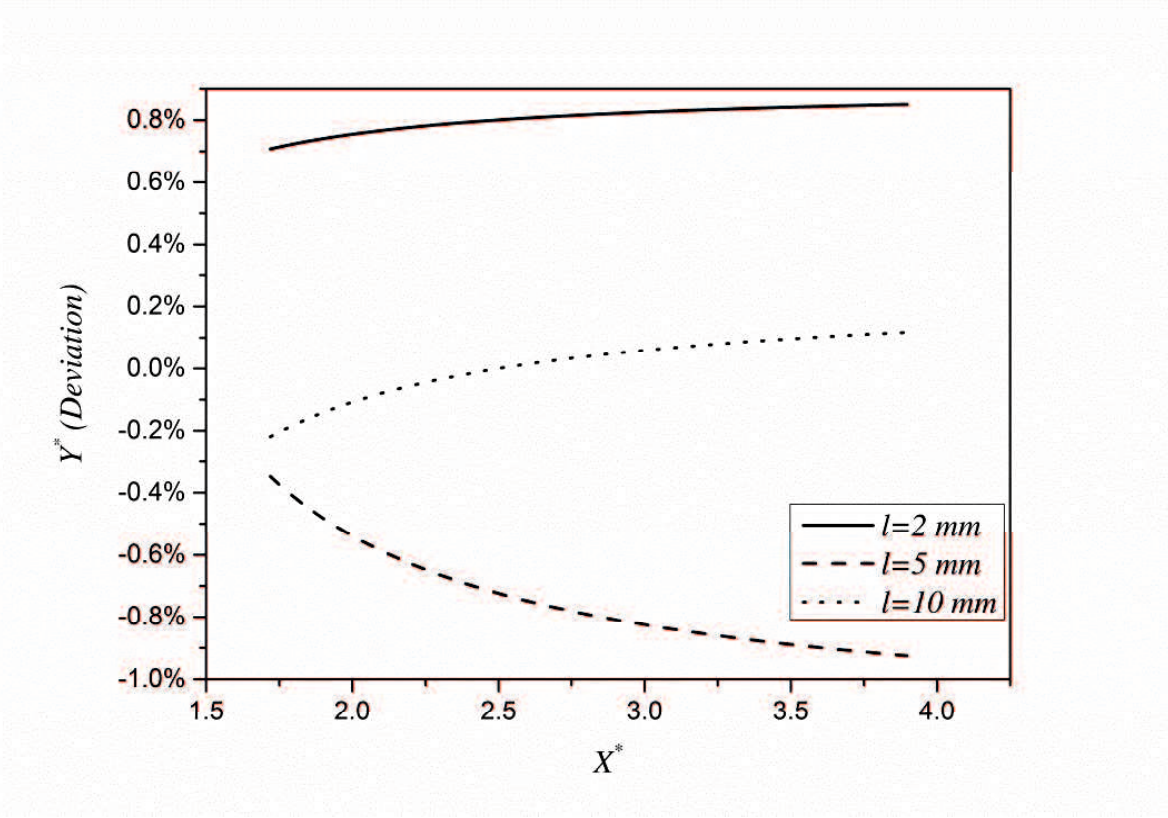

Fig. 5-3 Percentage deviation of the calibration curve obtained from the experimental data.

The sublayer plate is expected to be able to measure the local wall shear stress for almost the entire range of high-Reynolds-number wall turbulence providing the plate can be manufactured thin enough to remain in the viscous sublayer. In order to verify the universality of the calibration curve, based on the conclusion from the channel flow, we did the same experiment in a fully developed pipe flow. In the pipe flow, the plate was glued on the surface and the thickness (h=0.05mm and 0.1mm) was measured by a micrometer. The length of the plate is 5mm. The accuracy of measurement is of the order 1 micrometer. The pipe flow having 70mm diameter and 5,700mm length was confirmed as a standard one in which logarithmic velocity profile with Karman constant 0.41 and additive constant 5.0 (Thuyein, et al., 2010). As shown in Fig. 5-4, we compared the

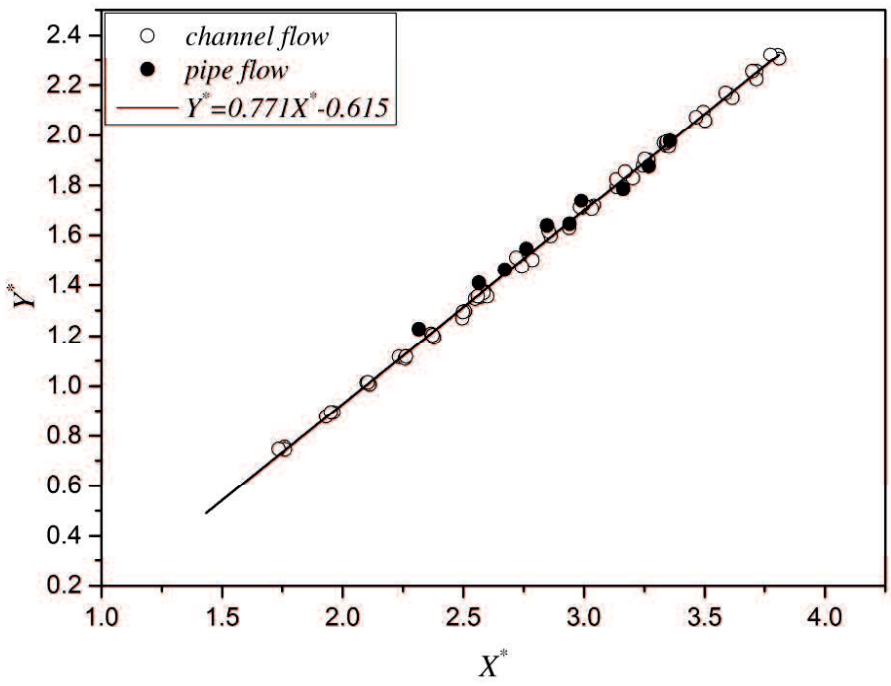

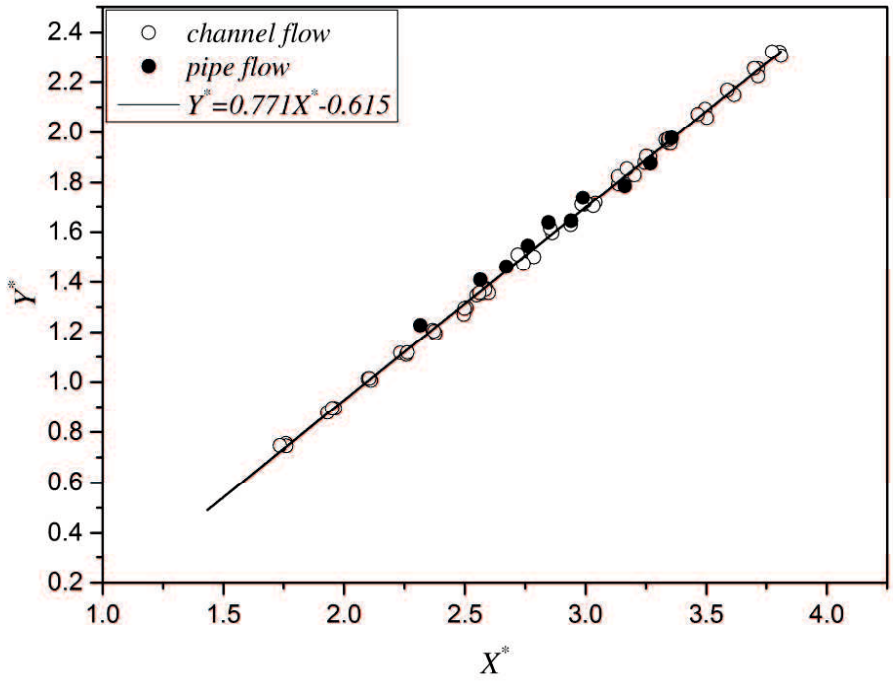

Fig. 5-4. Universal of the calibration curve for channel flow and pipe flow. The pipe flow is in fully developed condition in which the logarithmic velocity profile with Karman constant of 0.41 and additive constant of 5.0 (Thuyein, et al., 2010).

In the present study, the sensitivity of the sublayer plate is compared with experimental data (Higuchi, 1985 and Rechenburg, 1963) reported in a survey by Winter (1977). The sensitivity, which is defined as the ratio of the pressure difference to the wall shear stress, is compared with the sensitivities of the sublayer fence, the Preston tube, and the razor blade methods in Fig. 5-5. The Preston tube, which uses only the stagnation pressure, has a lower sensitivity at a smaller dimensionless height. At a smaller dimensionless height as compared to the wall, h+, the sensitivity of

the sublayer plate is as high as that of the sublayer fence. The deviation between sublayer plate and the sublayer fence is less than 2% in the linear sublayer. For both the sublayer fence and the sublayer plate, the use of negative pressure at the trailing edge is advantageous for pressure difference measurement at low Reynolds numbers. The experimental evidence indicates that the sensitivity of the sublayer plate is sufficient if the plate is enveloped by the linear sublayer.

It was unexpected that the sublayer plate has sensitivity as high as the sublayer fence. The fences likely make larger separation bubble and lower pressure behind it. However, the plate has almost same level of sensitivity as the plate and fence are submerged in the linear sublayer. When the edge of the fence and plate are in the buffer layer, the sensitivity of the plate is certainly lower than that of the fence. The facts suggest that behaviors of separation from edge are similar for the plate and fence if they were submerged in the linear sublayer. The flow is purely viscosity and any obstacles are supposed to be classified into hydrodynamically smooth (see e.g. Schlichting, 1979). As the fence and plate are submerged in the linear sublayer, it is fairly expected that the plate and fence can produce the same level of the pressure difference.

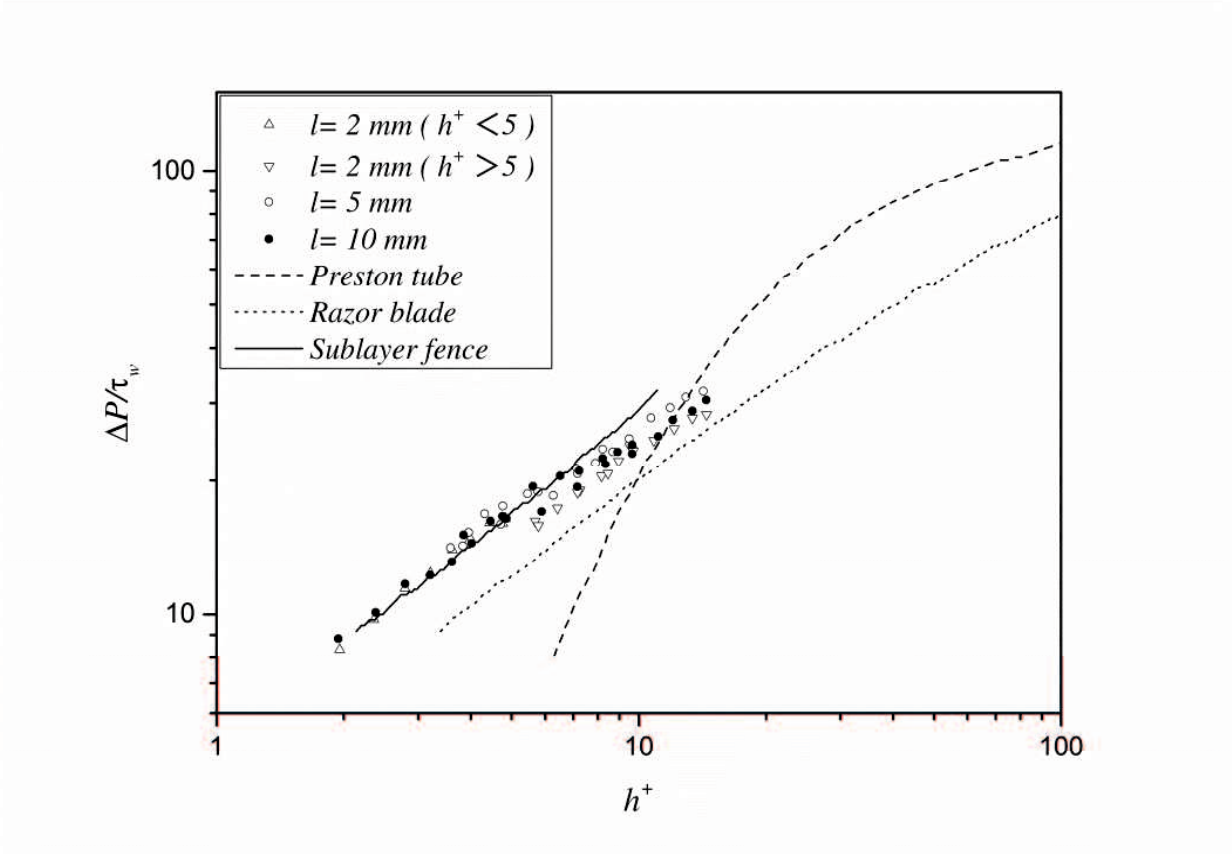

Fig. 5-5 Sensitivity of the sublayer fence, a razor blade, and a Preston tube. The lines of Preston tube, Razor blade and Sublayer fence are referred from the review reported by Winter (1977)

The finite spanwise width of the sublayer plate may affect the pressure measurement. The plate length and thickness were fixed at l = 2 mm and h = 0.2 mm, respectively, and the experiment was conducted at Re = 16,000. Four widths, 6, 8, 10, and 13.3 mm, corresponding to aspect ratios of 30, 40, 50, and 66.5, were investigated. Figure 5-6 shows the dependence on w/h of the measured pressure at the leading and trailing edges. The vertical axis indicates the change in pressure associated with

the sublayer plate installation position. In the figure, P is the pressure with the sublayer plate, and P_w is the standard wall static pressure without the sublayer plate. The aspect ratio does not appear to affect the stagnation pressure at the leading edge. When $w/h < 50$, the magnitude of the negative pressure at the trailing edge is reduced for a lower aspect ratio.

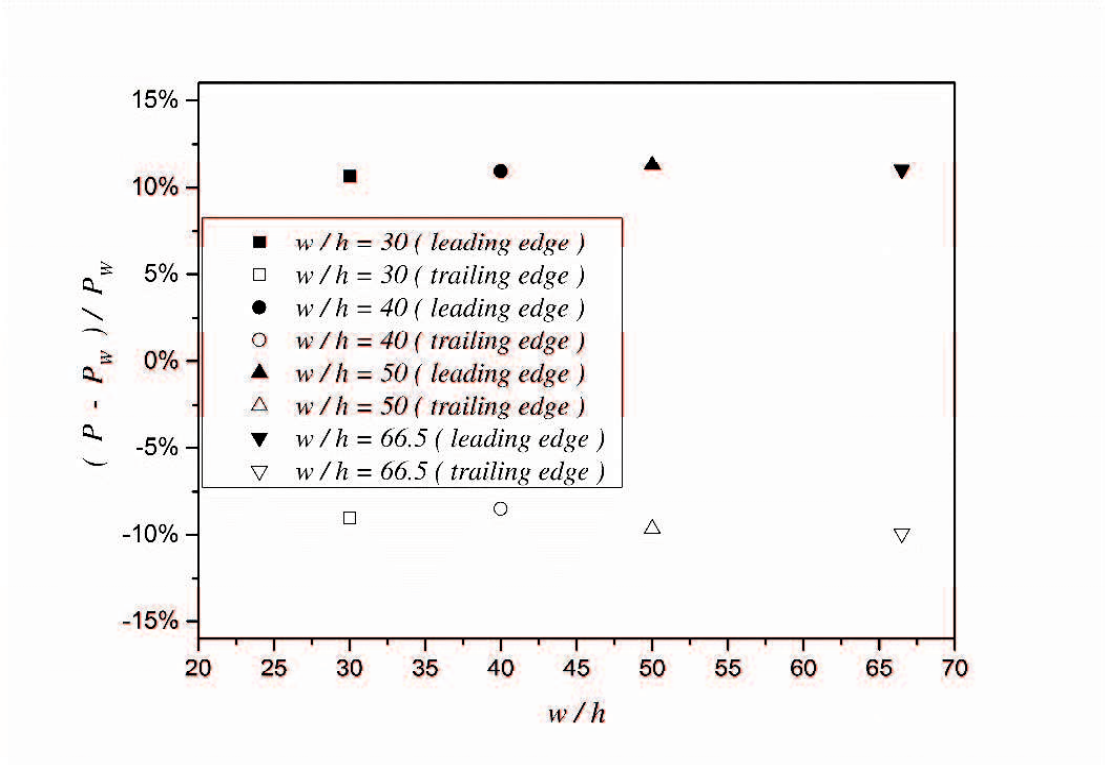

Fig. 5-6 Effect of plate width on the static pressure at the trailing and leading edges.

The sensitivities of these plates are plotted in Fig. 5-7 in the same manner as in Fig. 5-5. The narrower plates have slightly lower sensitivity and a lower pressure difference for the same wall shear stress and h+. Both edges of the plate usually generate longitudinal vortices, as was often observed in the flow around obstacles placed on the wall. These vortices

are referred to as necklace or horseshoe vortices, and the pair of longitudinal vortices induces a secondary current toward the wall just downstream of the obstacle (see, e.g., Lugt, 1983). The vortices are of the same order as the obstacle height. In the case of an insufficient spanwise width of the plate, the secondary current could reduce the magnitude of the negative pressure at the trailing edge of the plate. For a sufficiently larger spanwise width for $w/h > 50$, the longitudinal vortices do not affect the pressure at the centerline downstream of the obstacle.

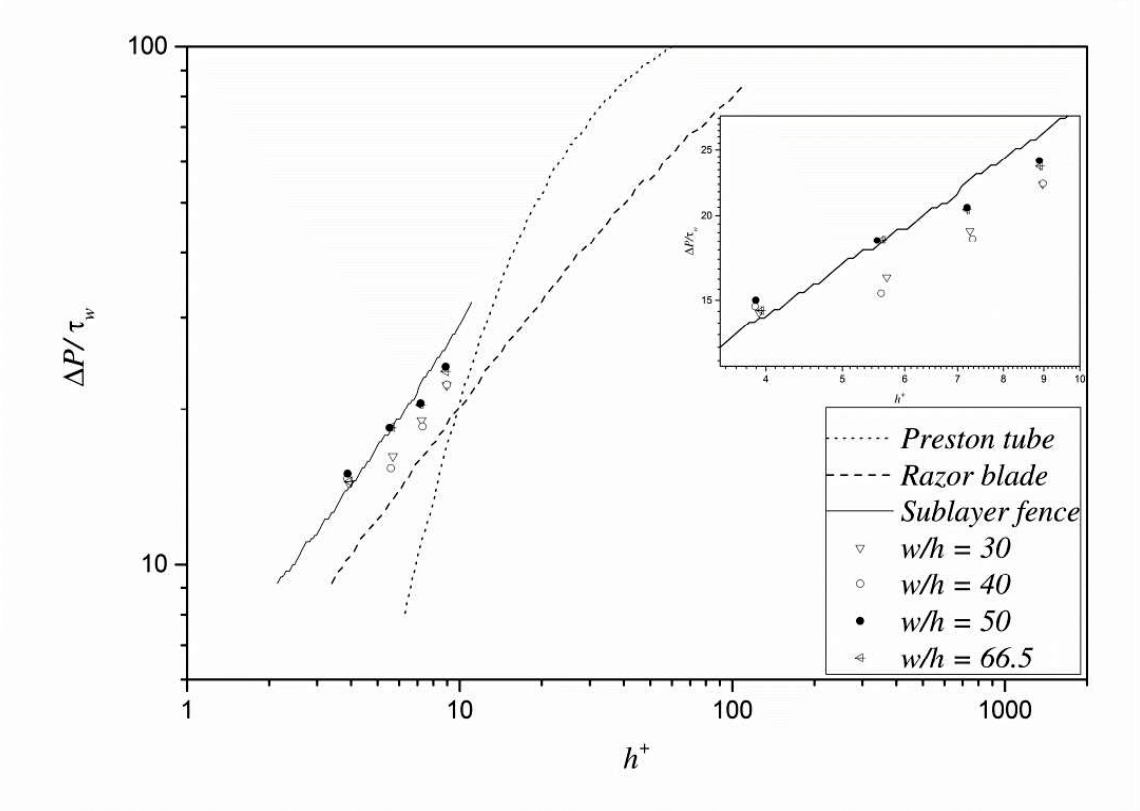

Fig. 5-7 Effect of plate width on dimensionless pressure sensitivity. Comparison is made in the same manner as in Fig.5-5.

The sublayer plate produces a stagnation pressure at the straight leading edge, as has been observed for the sublayer fence. The stagnation pressure is expected to depend on the angle of attack of the plate edge with respect to the wall shear stress or limited streamline orientation. This property could be used to detect the direction of the wall shear stress and limited streamline. The dependence of the pressure difference on the angle of attack of the plate with respect to the wall shear stress was examined experimentally for three plate lengths, l = 2, 5, and 10 mm, and two plate thicknesses, h = 0.1 and 0.3 mm. The plate width was maintained at greater than 50 times the plate thickness, and the experiment was conducted at Re = 16,000. The angle of attack was varied by rotating the plug on which the sublayer plate was mounted . The effect of the aspect ratio on the angular resolution was examined for plate lengths of 5 mm and 10 mm for h = 0.2 mm and w = 30 mm, and the obtained results are shown in Fig. 5-8. The pressure difference was normalized by a pressure difference at an angle of attack, α, of 0 degrees. The solid line represents the semi-empirical relation proposed for the sublayer fence by Vagt and Ferenholz (1973):

$$\frac{\Delta P_{\alpha}}{\Delta P_{n}} = \exp\left[-\left(1.025\frac{\pi}{180}\alpha^{\circ}\right)^{2}\right] \qquad 5.3$$

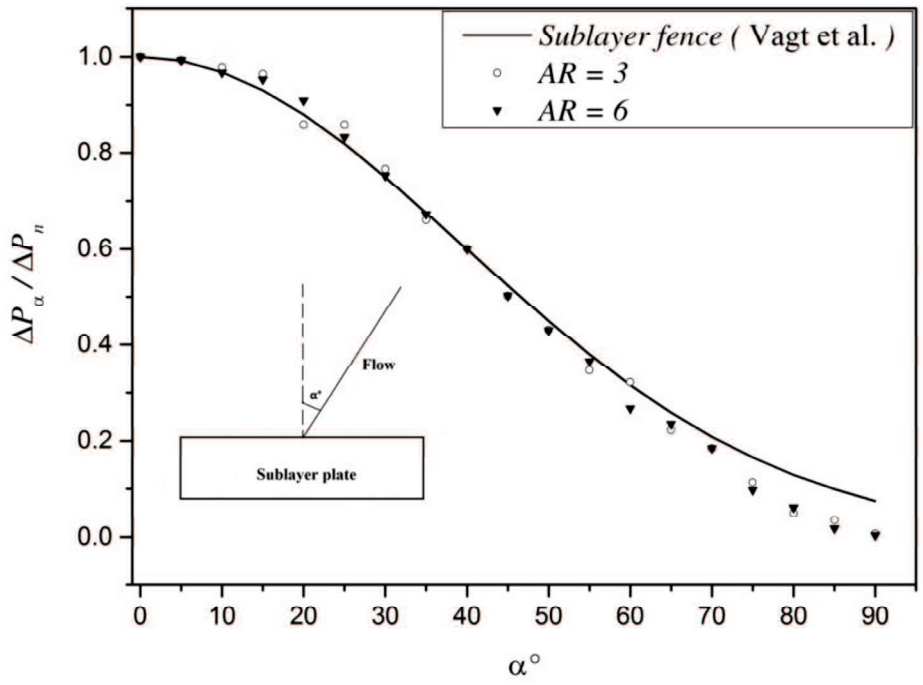

Fig. 5-8 Variation of pressure difference with yaw angle of attack for aspect ratios of 3 and 6. The solid line represents the semi-empirical formula for the sublayer fence reported by Vagt and Fernholz (1973).

The sublayer plate has approximately the same dependence on the stagnation pressure as the semi-empirical relation proposed for the sublayer fence at angles of attack of less than 60 degrees. The experimental data for AR = 3 and AR = 6 agree well with the sublayer fence up to attack angles of less than 60º (the percentage error less than ±4%).

5-3 Circular plate

At first, we want to propose the measurement procedure of sublayer plate using circular sublayer plate. Once the circular sublayer plate is calibrated, the following procedure can be used for a measurement within an unknown, three dimensional boundary layer: first, the sublayer plate is placed on the test wall surface.(as shown in Fig. 4-10) The pressure difference ΔP is recorded (as shown in Fig.5-9) and the pressure difference around the edge (as shown in Fig.5-14) is recorded. The direction of wall shear stress, α, is determined from Fig. 5-14. Finally, from Fig.5-10, the magnitude of the wall shear stress is determined.

In the sublayer plate method, a simple thin rectangular plate is attached to a wall with two wall static pressure taps. The plate can easily be fabricated to have the exact same size and shape, and can be used to calculate the wall shear stress using a universal calibration curve. The sublayer plate also has the ability to detect the flow direction, namely, the direction of limited streamlines on the wall. In the present experimental study, the feasibility of using a sublayer plate to detect the flow direction with higher accuracy will be examined in a canonical two-dimensional turbulent channel flow. Considering the ratios of the static wall pressure

measurement values, a circular sublayer plate with multiple static pressure taps will be used as the sublayer plate. The round edge of the plate could reduce the absolute values of the stagnation pressure at the upstream edge of the plate and the negative pressure at the downstream edge of the plate. The influence of the curvature of the round edge on static pressure measurement will be discussed, and, based on experimental results, we propose an arrangement of the plate and pressure taps that enables the flow direction to be determined with much higher accuracy.

In a previous experiment, $\Delta x = 0.15$ mm was confirmed to be the best gap size for the rectangular sublayer plate. In the present study, the first step was to optimize the gap size for the circular plate. At Re = 16,000, the gap size was varied from 0.03 to 0.3 mm, with an accuracy of ±0.005 mm. The influence of round edge of the plate on the pressure measurement was examined for pressure taps in front of the plate ($\alpha = 0^0$) and behind the plate ($\alpha = 180^0$). Figure 5-9 shows the static pressure at the leading and trailing edges of the circular plate, and includes the data for the rectangular plate for comparison. The vertical axis is the relative pressure difference with respect to the wall pressure without the plate. For both the circular and rectangular plates, this value is positive due to flow stagnation at the

leading edge ($\alpha = 0^0$) and is negative due to flow separation at trailing edge ($\alpha = 180^0$). The circular plates produce smaller relative differences compared to the rectangular plates. The round edge of the circular plate reduces the magnitude of the pressure difference and the sensitivity for the wall shear stress measurement.

The relative pressure difference remains approximately constant in the range Δx = 0.05 to 0.25 mm (Δx/d = 0.17 to 0.83) for all circular and rectangular plates. The influence of the gap size on the pressure measurement is also small for the circular sublayer plate. The gap size Δx = 0.15 mm is applicable to the circular plate.

The wall shear stress measurement results for the circular plate must be checked by comparison with calibration curves. Calibration curves must be determined as a functional relation between two dimensionless quantities derived from dimensional arguments, in a manner similar to that for a Preston tube or a sublayer fence, as follows:

$$Y^* = \log(\tau_w h^2 / \rho\nu^2) \quad \text{and} \quad X^* = \log(\Delta P h^2 / \rho\nu^2) \qquad 5.4$$

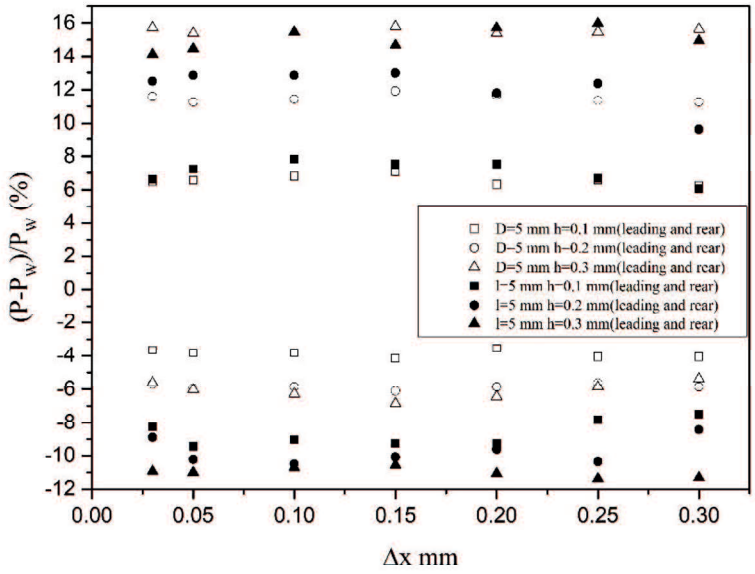

(a)

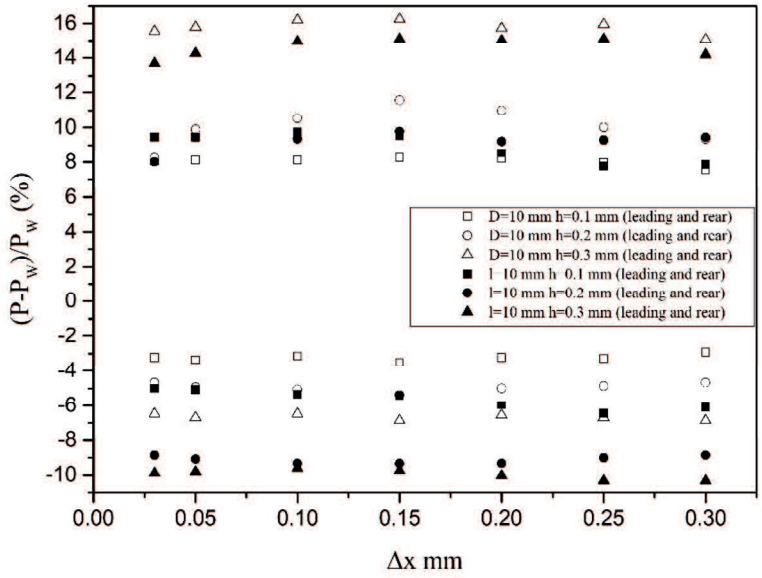

(b)

Fig. 5-9 Static pressure at the leading and trailing edges of the plate as a function of the gap between the plate and the pressure gap. (a) Comparison between the circular plate *D* = 5 mm and the rectangular plate *l* = 5 mm. (b) Comparison between the circular plate *D* = 10 mm and the rectangular plate l = 10 mm.

The functional relation between the two dimensionless quantities for three plate thicknesses (h = 0.1, 0.2, and 0.3 mm) is plotted for D = 5 and 10 mm in Fig. 5-10. The figure also shows the calibration curves for the circular plate and the rectangular plate. The dashed line indicates a universal calibration curve obtained using a rectangular plate . The straight line indicates the relation obtained by the least-squares method for all experimental data for circular plates of three sizes, with D = 5 and 10 mm. The experimental results can be well represented by the calibration curves calculated without any clear differences associated with the thickness of the plate:

D = 5 mm:

$$Y^* = 0.755X^* - 0.496 \quad 1.65 < X^* < 3.76 \qquad 5.5$$

D = 10 mm:

$$Y^* = 0.781X^* - 0.599 \quad 1.74 < X^* < 3.76 \qquad 5.6$$

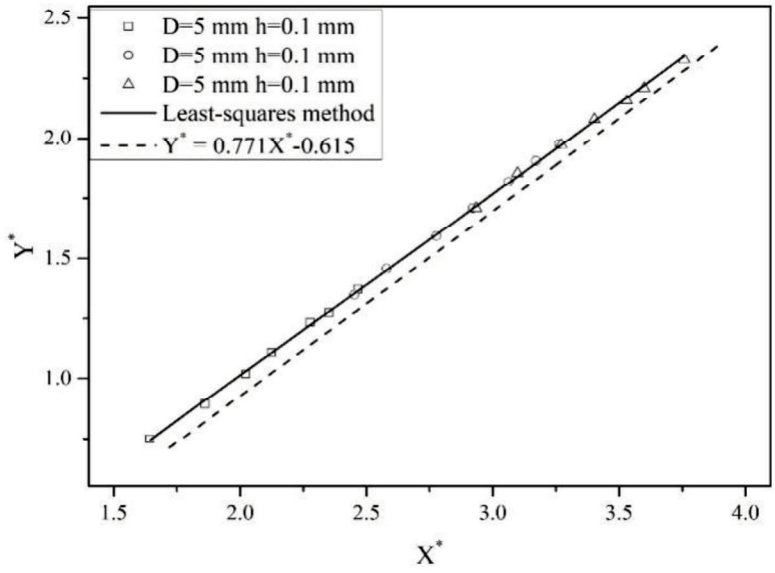

(a)

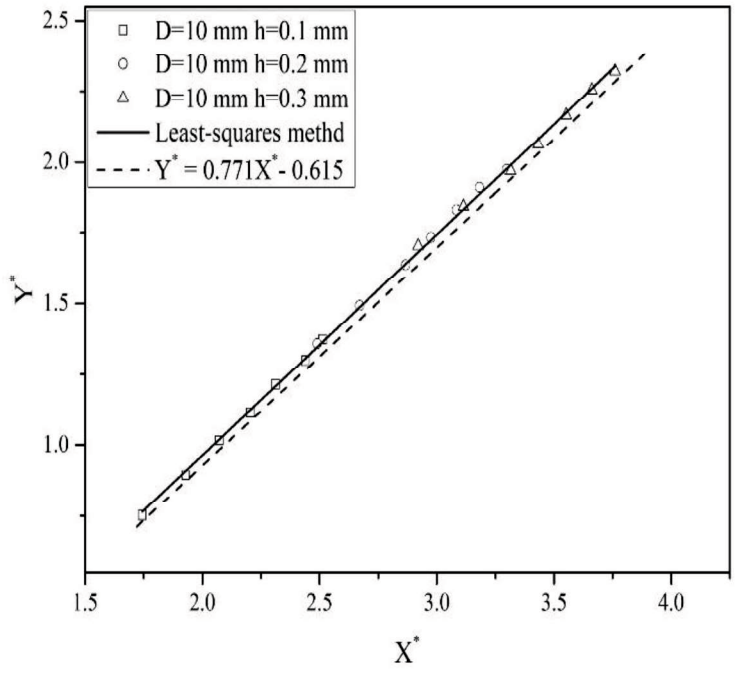

(b)

Fig. 5-10 Calibration curves for three parameters obtained from experimental data for the circular plate (solid lines) and the rectangular plate (dashed line). (a) D = 5 mm, (b) D = 10 mm. The solid lines were obtained by Equations (5.5) and (5.6), respectively.

The calibration curve depends slightly on the diameter of the plate, i.e., the curvature of the plate edge. The circular plates produce smaller X* values for a given Y* in comparison to the rectangular plates. This means that the pressure difference for the circular plates is smaller at the same wall shear stress and plate thickness. The deviation between the calibration curve for D = 5 mm and the calibration curve for the rectangular plate is 2.07%. Moreover, the deviation between the calibration curve for the circular plate with D = 10 mm and that for the rectangular plate is 1.29%. The equation for the larger diameter, D = 10 mm, is closer to the universal curve determined using a rectangular plate. For the same plate thickness, the circular plate with a diameter D = 10 mm has a smaller difference in sensitivity to that for the rectangular plate, as compared with the circular plate with a diameter of D = 5 mm. The larger curvature of the plate with a smaller D has a larger influence on the lower magnitude of the stagnation pressure at the leading edge and the separation at the trailing edge.

In the present study, the sensitivity of the circular sublayer plate was compared with the available experimental data (Higuchi, 1985 and Rechenberg, 1963) reported in a survey by Winter (1977). The sensitivity, which is defined as the ratio of the pressure differences to the wall shear stress, is compared with the sensitivities for the rectangular sublayer plate, the sublayer fence, and the razor blade methods in Fig. 5-11.

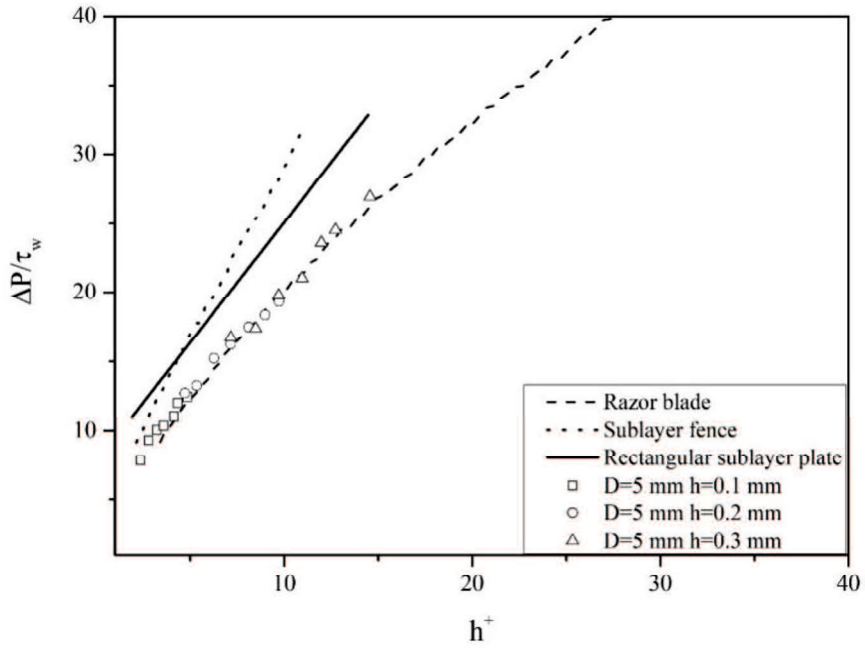

(a)

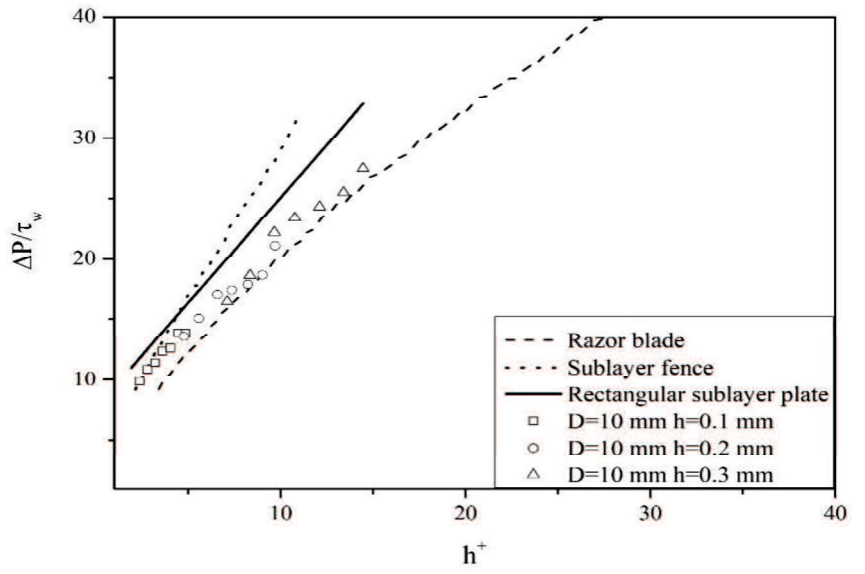

(b)

Fig. 5-11 Sensitivity of the sublayer fence, the razor blade, the sublayer plate, and the circular plate. The lines for the razor blade and the sublayer fence were obtained from Winter (1977). The line for the rectangular sublayer plate was obtained from Hua, Suzuki, and Mochizuki (2017). (a) D = 5 mm, (b) D = 10 mm.

For a smaller dimensionless height from the wall, h+, the sensitivity of the circular plate method with D = 5 mm is as high as that of the razor blade method. The difference between the sensitivities of the circular plate and razor blade methods is less than 2% in the linear sublayer, $h^+ < 5$ (Schlichting, 1979). For a smaller dimensionless height from the wall, $h^+ <$ 3 to 5, the sensitivity of the circular plate method with D = 10 mm is as high as that of the rectangular sublayer plate and the sublayer fence methods. When h^+ approaches 10, corresponding to the buffer layer height, the sensitivity of the circular plate method with D = 10 mm is as low as that of the razor blade method. In the limited case in which the circular sublayer plate is submerged in the linear sublayer and D is sufficiently large, the round edge of the circular plate has a small influence on the pressure difference measurement.

A circular sublayer plate with eight pressure taps was designed and fabricated while referring to the shear stress vector sensor proposed by Hakkinen et al. (2003) (see Fig. 5-12). Eight static pressure taps with diameters of 0.3 mm were set with a gap of Δx = 0.15 mm around the edge at 45° increments. The diameter and thickness of the circular plate were 10 mm and 0.2 mm, respectively. The plate with h = 0.2 mm was thicker than the linear sublayer, i.e., the plate was located in the buffer layer for all conditions. The plate with h = 0.1 mm was thinner than the linear sublayer

only at low Reynolds numbers. It is undesirable for the sublayer plate to be thicker or thinner than the linear sublayer thickness for the investigation of its angular response. The circular sublayer plate with D = 10 mm and h = 0.2 mm was used to test the ability to detect the shear stress direction.

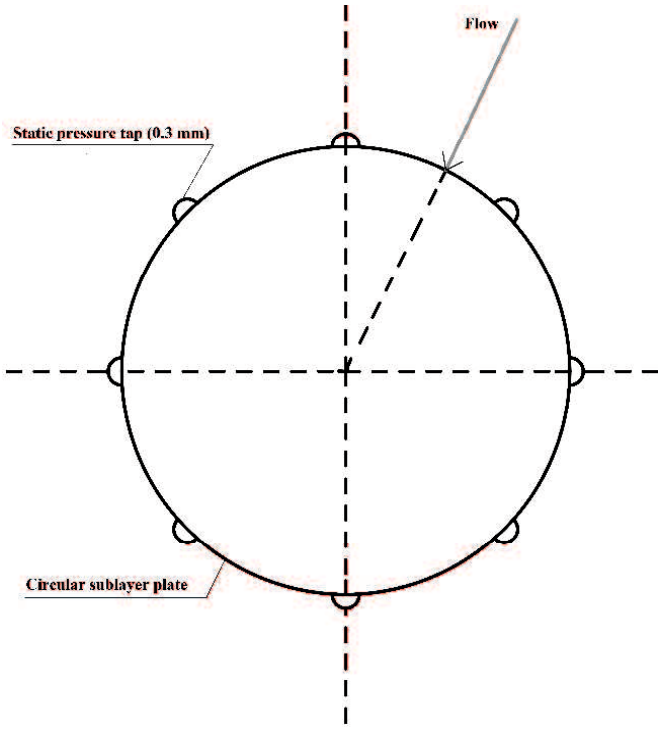

Fig. 5-12 Schematic diagram of the circular sublayer plate with eight pressure taps.

First, the pressure response at a single pressure tap was investigated for various directions of wall shear stress. Figure 5-13 shows the pressure measurement responses with a circular sublayer plate and a rectangular sublayer plate. The diameter and spanwise width were 10 mm, and the plate thickness was 0.2 mm. The measured wall pressure difference is normalized by the pressure difference ΔP_n at $\alpha = 0^0$. The dashed line

represents the semi-empirical relation proposed for the sublayer fence by Vagt and Fernholz (1973):

$$\frac{\Delta \boldsymbol{P}_{\alpha}}{\Delta \boldsymbol{P}_{\boldsymbol{n}}} = \mathbf{exp}\left[-\left(1.025\frac{\pi}{180}\alpha^{\circ}\right)^{2}\right] \qquad 5.7$$

The solid line represents the semi-empirical relation proposed for the circular sublayer plate:

$$\frac{\Delta P_{\alpha}}{\Delta P_{n}} = 1 - 1.6\times10^{-3}\alpha - 3.21\times10^{-4}\alpha^{2} + 2.02\times10^{-6}\alpha^{3}, \quad \alpha = 0 \text{ to } 90^{\circ} \qquad 5.8$$

The semi-empirical relation given by Vagt and Ferenholz(1973) fails to represent the angular response of the circular sublayer plate. The curvature of the circular plate probably generates a spanwise current near the rounded plate edge and influences the angle of attack of the approaching flow. However, a cubic function fits the experimental data very well for $\alpha = 0$ to 90°. Appropriate fitting of the analytic function for a wide range of flow directions can be useful in detecting the wall shear stress vector.

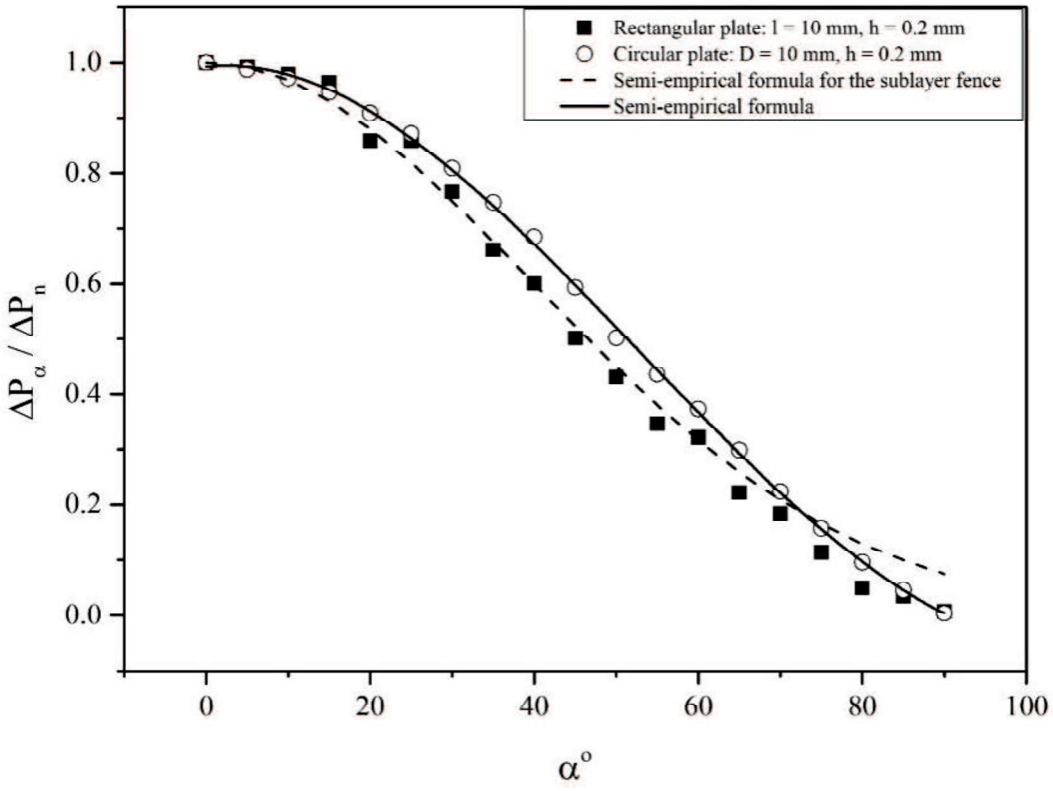

Fig. 5-13 Pressure differences with yaw angle of attack for the rectangular plate (■) and circular plate (○). The solid line was obtained by the semi-empirical formula of Equation 5.8. The dashed line indicates the semi-empirical formula of Equation 5.7 for the sublayer fence reported by Vagt and Fernholz (1973).

Regarding the measurement of the wall shear stress, the measurement range covered by one static pressure tap is a deflection angle of $\alpha = 0$ to $\pm 22.5^0$, so the measurement is performed in increments of 5° over a deflection angle range of $\alpha = 0$ to 20^0. In order to achieve a higher detection accuracy, we consider the ratio of the pressure differences at two taps neighboring the tap with the maximum stagnation pressure. Regarding the measurement method using the eight-tap plug, the indicated pressure for

each static pressure tap is defined as $P_1 > P_2 > P_3 > ... > P_7 > P_8$ (see the upper part in Fig. 5-14). The directional characteristics for the pressure measurement are shown for $\alpha = \pm 90^0$ with respect to P_1 for the main flow direction $\alpha = 0^0$. The indicated pressure is relatively constant within the range of $\alpha = +90^0$ to -90^0 on the downstream side. Therefore, the indicated pressures P_6, P_7, and P_8 are set to the backward stagnation pressure P_B, and the pressure difference from P_1 to P_3 is set as $\Delta P_1 (=P_1-P_B)$ to $\Delta P_3 (=P_3-P_B)$. As shown in Fig.11, there are two static pressure taps to detect the instructed pressure P_2 and P_3. The position of the static pressure tap is closed to 45^0 with respect to the flow direction. There is the deflection angle between P_1 and flow direction. That was used to determine the direction of the shear stress indicated by the difference of these pressures. Using these definitions, it can be considered that it is possible to obtain a deviation angle α with respect to the static pressure tap of P_1 located between the two static pressure taps. Therefore, in the present study, the deflection angle α is obtained as the ratio of ΔP_2 and ΔP_3.

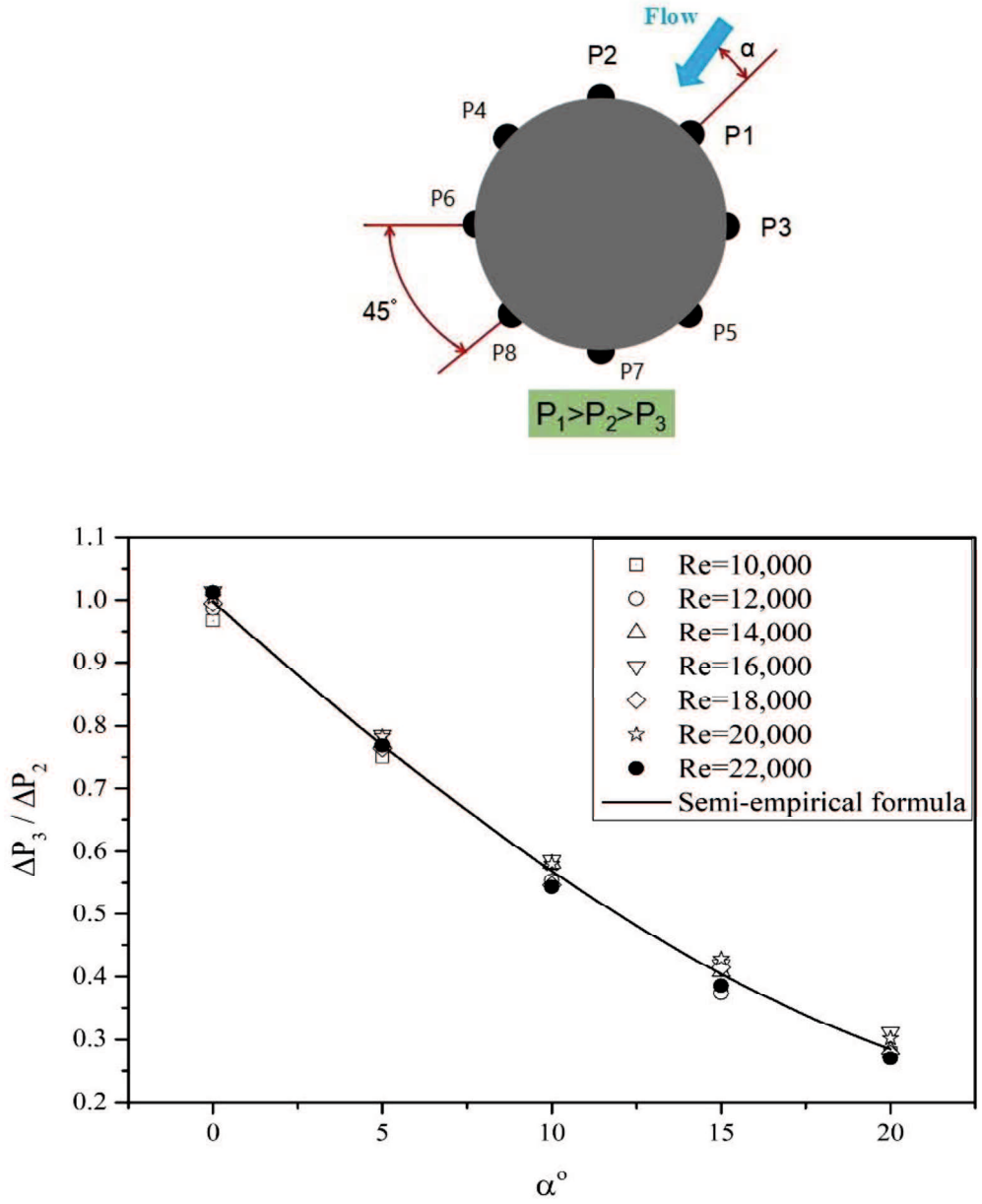

Fig. 5-14 Direction measurement using the pressure ratio between the two taps adjacent to the maximum-stagnation-pressure tap at Reynolds numbers of 10,000, 12,000, 14,000, 16,000, 18,000, 20,000, and 22,000. The solid line is given by Equation 5.9 . The upper figure shows the pressure tap arrangement for the maximum stagnation pressure P_1 and the pressures P_2 and P_3 at the two neighboring taps.

Figure 5-14 shows $\Delta P_3/\Delta P_2$ at each Reynolds number with respect to the deflection angle α. The approximate curve at a deflection angle of α = 0 to 20° is indicated by the solid line.

$$\frac{\Delta P_3}{\Delta P_2} = 1 - 0.05 \times \alpha + 3.68 \times 10^{-4} \times \alpha^2 + 1.18 \times 10^{-5} \times \alpha^3,$$

$$\alpha = 0 \text{ to } 20^{o} \qquad 5.9$$

The solid line successfully represents the experimental data for α = 0 to 20º. The variation of the pressure difference ratio is considerably larger than that for the surface block [9]. The circular sublayer plate with eight pressure taps can measure the wall shear stress vector with higher sensitivity with respect to magnitude and direction for 360º. In other words, when conducting experiments under the condition that this relationship holds, a simple method (circular sublayer plate) of measuring the skin friction vector can be deduced that does not require preliminary measurement of the vector direction.

Chapter 6

Conclusions

A local wall shear stress measurement technique involving a sublayer plate was proposed in order to determine the local wall shear stress using an easily fabricated device, and experiments were conducted in order to investigate the accuracy and angular resolution in a canonical wall turbulent flow, namely, a fully developed two-dimensional turbulent channel flow.

The calibration curve generated by the two dimensionless parameters is independent of the specifications of the rectangular plate and is not affected by the finite length of the plate, the streamwise length, or the spanwise width. The sensitivity of the rectangular sublayer plate is as high as that of the sublayer fence if they were submerged in the linear sublayer. If the plate is enveloped by the linear sublayer, the sublayer plate can produce a pressure difference sufficient for accurate measurement of the local wall shear stress. The angular resolution of the rectangular sublayer plate is represented in the same manner as that of the sublayer fence. It is expected that the sublayer plate can be used to detect

the direction of the wall shear stress. Based on the comparison of plates of various sizes, the plate width should be greater than respectively 50 times the thickness of the sublayer plate. Note that, unlike the sublayer fence, the sublayer plate is easily fabricated. A unique calibration curve must be obtained in a canonical flow field for each individual sublayer fence. In contrast, sublayer plates can be used for wall shear stress measurement using a universal calibration curve, as with the Preston tube method.

The calibration curve generated by the two dimensionless parameters depends weakly on the specifications of the circular plate in the linear sublayer. The sensitivity of the circular plate is reduced slightly in comparison with the rectangular plate. If a circular sublayer plate of sufficiently large diameter is submerged in the linear sublayer, the sensitivity remains approximately the same as that for a rectangular sublayer plate. A cubic semi-empirical function fits the experimental data extremely well for a wide range of wall shear stress angles of $\alpha = 0$ to 90°. A circular sublayer plate with eight pressure taps was designed and tested in order to detect the wall shear stress vector in a situation in which the flow direction is initially unknown. The ratio of the pressure differences at two taps neighboring the tap with the maximum stagnation pressure provides higher angular resolution in comparison with the surface block gage and can detect the wall shear stress vector over 360º. The circular

sublayer plate with 8 pressure taps can measure wall shear stress vector in complicate wall turbulence subjected to pressure gradient or cross stream current such as flow on the aircraft wings.

Acknowledgements

The work in this thesis has been carried out, mainly in the Laboratory for Fluid Machines, Mechanical Department, at Yamaguchi University, Japan. Many people have been involved in the work and I am very grateful for their help, but there are some persons I want to thank especially.

In the first place, I would like to express my gratitude to my supervisor, Prof. Shinsuke Mochizuki for his intellectual and moral support over the past four years. It has been a great pleasure to work under his professional guidance in the field of mechanics and turbulence, for clarifying discussions on the analysis of the boundary layer, and to be inspired by his positive attitude through the best and the worst of times. Meanwhile, I would like to thank Prof. Li Qinggang in Xihua University, China, for giving me the opportunity to go to study and work in Yamaguchi University and for his insightful comments during various stages of studying in China. In the same time, I would like to thank Dr. Hiroki Suzuki for his advice and guidance in this work. Nevertheless, I would like to thank Prof. Liu in North China Electric Power University, China, for guiding my first steps in fluid scientific field and also for all the knowledge they thought me during my university years.

I wish to thank Mr. Kishii and Mr. Nakayama for carefully carrying out the experiment and for their help with designing many of the mechanical components used in experiments.

My collaboration with the other students and doctors has been thoroughly enjoyable and helped me in acquiring a great learning experience. I have made some really good friends, during my stage in the Laboratory for Fluid Machines, China and Japan. I am thankful to all of them (especially to Shinya Hiramatsu) for a pleasant, stimulating and inspiring atmosphere, as well as for their friendship.

I would like to thank to my girlfriend, Dr. Cao Yuan, for her encouragement, understanding since the beginning of my thesis. I am especially grateful to her.

Last but not the least, I would like to thank, from all my heart, to my family for their moral support and encouragement throughout my educational career. My parents have made innumerable sacrifices for my education and I find it difficult to express my gratitude in just a few words. As a tribute, I dedicate this thesis to them.

Reference

Allen, J.M. (1976), Systematic study of error sources in skin friction balance measurements, NASA TN- D-8291.

Antonia, R.A., Teitel, M., Kim, J. and Browne, W.B. (1992), Low-Reynolds-number effects in a fully developed turbulent channel flow, J. Fluid Mech., 236: 579-605.

Bandyopadhyay, P.R. and Weinstein, L.M. (1991), A refection-type oil-film meter, Exp. Fluids, 11: 281-292.

Barenblatt, G., Chorin, A., Hald, O., and Prostokishin, V. (1997a). Structure of the zero-pressure-gradient turbulent boundary layer. In Proc. Natl. Acad. Sci. USA, Applied Mathematics, volume 94, pages 7817–7819.

Clauser, F. (1954). Turbulent boundary layers in adverse pressure gradients. In Aero. Sci., volume 21, pages 91–108.

Dean, R. B. (1978), "Reynolds number dependence of skin friction and other bulk flow variables in two-dimensional rectangular duct flow", Transactions of the ASME, J. Fluids Eng., 100: 215-223.

Dextor, P. (1974), Evaluation of a skin-friction vector-measuring instrument for use in 3-d turbulent incompressible boundary layers., University of Southampton Department of Astronautics and Aeronautics Undergraduate project.

Fernholz, H., Janke, G., Schober, M., Wagner, P., and Warnack, D. (1996). New developments and applications of skin-friction measuring techniques. Meas. Sci. Technol.,7:1396–1409.

Gupta, R. P. (1975), A new device for skin-friction measurement in three-dimensional flows, AIAA J. 13-2, 236-238.

Gasser, D., Thomann, H., and Dengel, P. (1993). Comparison of four methods to measure the wall shear stress in a turbulent boundary layer with separation. Exp. Fluids, 15:27–32.

Goldstein (1965), Modern Development in Fluid Dynamics, Vol.1, Dover Publ., 1965.

Hanratty,JA, Campbell, Goldstein, R.J(1983), Fluid Mechanics Measurements, Hemisphere, 559-615.

Hakkinen, R. (1991). Survey of skin friction measurements techniques. AIAA Mini-symposium

Higuchi, H.(1985), “A miniature, directional surface-fence gage”, AIAA Journal, 23-8, 1995-1196.

Hakkinen, R.J., Neubauer, J.S., Hamory, P.J., Bui, T.T. and Noffz, G.K., (2003), Exploratory calibration of adjustable-protrusion surface-obstacle (APSO) Skin Friction Vector Gage, AIAA, NASA/TM-2003-210739

Kalvesten, E. (1995). Pressure and wall shear stress sensors for turbulence measurements. PhD thesis, Royal Institute of Technology, Stockholm, Sweden.

Ligrani, P. M. and Bradshaw, P.(1987), Spatial resolution and measurement of turbulence in the viscous sublayer using subminiature hot-wire probes, Exp. Fluids, 5-6: 407-417.

Lugt, H. J.(1983), Vortex Flow in Nature and Technology, University of California, John Wiley & Sons Inc. 85-87.

Mochizuki, S., Fukunaga, M., Kameda, T. and Sakurai, M., Sublayer plate method for local wall shear stress measurement, 19th Australia Fluid Mechanics Conference, Melbourne, Australia, 8-11, Dec., 2014.

Munson, Bruce R., at. al. Fundamentals of Fluid Mechanics, 2nd Edition. New York: John Wiley and Sons, 1994.

Nagib, H.M. and Chauhan, K.A.(2008), Variations of von Karman coefficient in canonical flows, Phys. Fluids, 20-101518: 1-10.

Osaka, H., Kameda, T. and Mochizuki, S.(1998), Re-examination of the Reynolds-number-effect on the mean flow quantities in a smooth turbulent boundary layer, JSME international Journal, 41-1: 123-129.

Prandtl, L. (1904). Uber Fl¨ussigkeitsbewegung bei sehr kleiner Reibung. ¨ Verh. III. Intern. Math. Kongr., Heidelberg, 1904, S. 484–491, Teubner, Leipzig, 1905.

Prandtl, L. (1932). Zur turbulenten stroemung in rohren und laengs platten. In Ergeb. Aerodyn. Versuch., 4, pages 18‑29, Goettingen.

Patel, V. C.(1965), “Calibration of the Preston tube and limitations on its use in pressure gradients”, J. Fluid Mech., 23-1: 185-208.

Preston, J. H.(1954), “The determination of turbulent skin friction by means of pitot tubes”, J. the Royal Aeronautical Society, 58: 109-121.

Rechenberg, I.(1963), “Messung der turbulenten Wandschubspannung”, Zeitschrift für Flugwissenschaften, 11-11: 429-438.

Schlichting, H. (1979), “Boundary layer theory, McGraw-Hill, New York 7th ed.: 616-617.

Thuyein A.W., Mochizuki, S. and Kameda, T. (2010), Response of fully developed pipe flow to rough wall disturbances (Mean velocity field), Journal of Fluid Science and Technology, 5-2: 340-350.

Vagt, J. D. and Fernholz, H. (1973), “Use of surface fences to measure wall shear stress in three-dimensional boundary layers”, Aeronautical Quarterly 24-2: 87-91.

Wei, T. and Willmarth, W.W. (1989), Reynolds-number effects on the structure of a turbulent channel flow, J. Fluid Mech., 204: 57-95.

Winter, K. G. (1977), An outline of the technique available for the measurement of skin friction in turbulent boundary layers, Prog. Aerospace Sci., 18-1: 1-57.

.